UNIWERSYTET WARSZAWSKI
WYDZIAŁ GEOLOGII

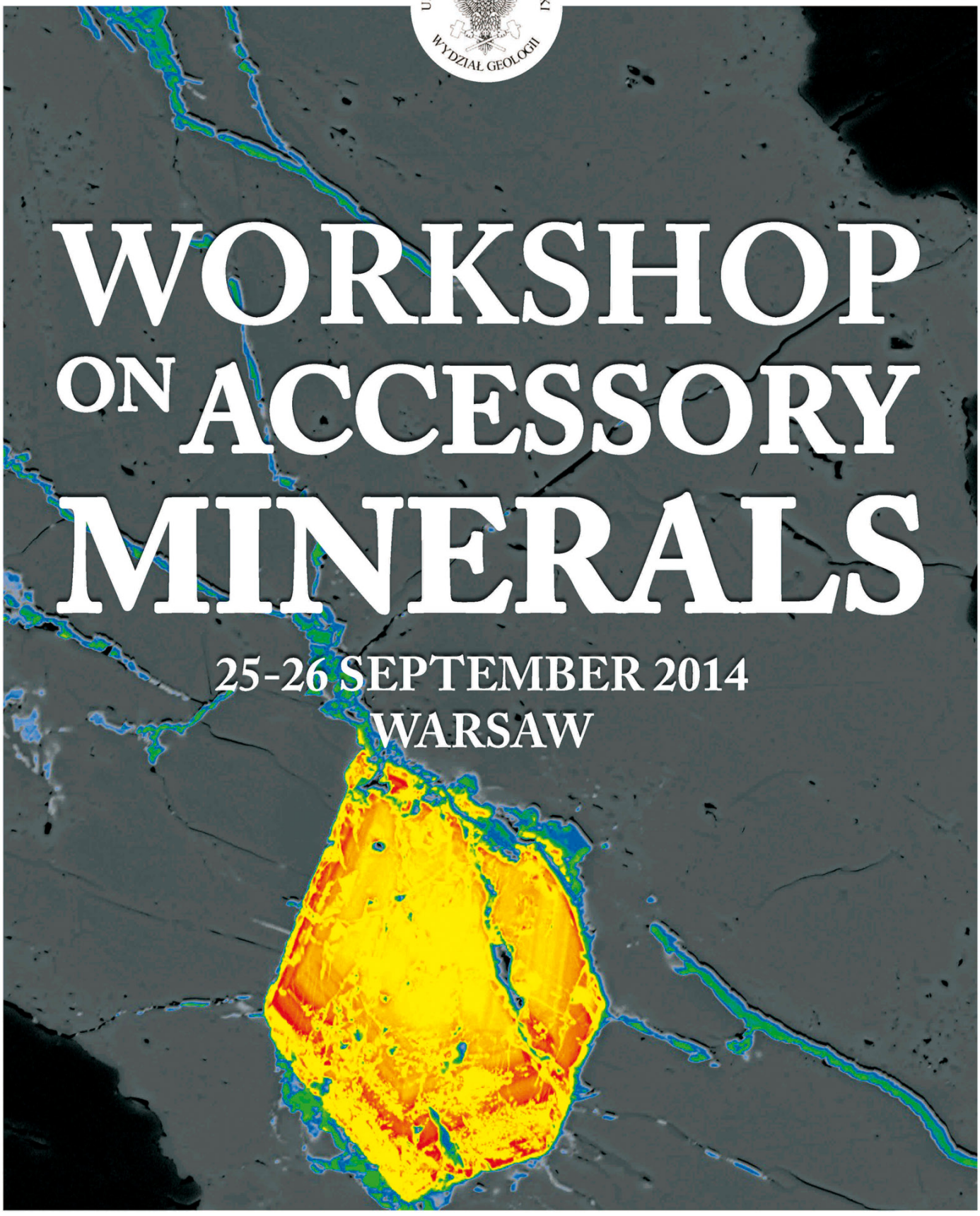

WORKSHOP ON ACCESSORY MINERALS

25-26 SEPTEMBER 2014
WARSAW

Workshop was financially supported by the Polish Ministry of Science and Higher Education subvention and research grant no N N307634040 and the Polish Geological Institute (PIG-PIB)

Cover photo: A euhedral, oscillatory zoned, primary monazite has been altered at the rims and along cracks to an allanite-apatite-xenotime assemblage. The host mineral is feldspar. Granite, Strzegom Massif.

Workshop on accessory minerals, University of Warsaw, September *2014*

Editors of Volume
Bogusław BAGIŃSKI, Oliwia GRAFKA Witold MATYSZCZAK,
Ray MACDONALD
Institute of Geochemistry, Mineralogy and Petrology, University of Warsaw
Al. Żwirki i Wigury 93, 02-089 Warszawa
b.baginski@uw.edu.pl

Language correction:
Ray MACDONALD
Institute of Geochemistry, Mineralogy and Petrology, University of Warsaw
Al. Żwirki i Wigury 93, 02-089 Warszawa
r.macdonald@lancs.ac.uk

Organizing committee:

Bogusław BAGIŃSKI

Ray MACDONALD

Michał RUSZKOWSKI

Financial support: Workshop on accessory minerals was financially supported by the Polish Ministry of Science and Higher Education subvention and research grant No N N307634040, Faculty of Geology University of Warsaw and PIG-PIB.

Preface

The progress made over the past two decades in our understanding of accessory minerals containing HFSE has been remarkable. Even when "fresh-minted", minerals such as monazite, xenotime, allanite and zircon are compositionally and structurally complex. The complexity increases many times during low-temperature alteration processes, such as interaction with hydrothermal fluids and weathering. Progress has, of course, been expedited by the introduction of a range of exciting new technologies, especially in structure determinations.

On re-reading the excellent 2002 review of accessory mineral research by Poitrasson *et al*., one is struck by how far the subject area has advanced in 12 years. We felt that this was an opportune time to bring together a group of Earth scientists with special expertise in accessory minerals to outline their current research interests, to share ideas and to consider productive future research directions. We look forward to a set of stimulating, lively debates.

Ray Macdonald and Bogusław Bagiński

Reference

Poitrasson, F., Hanchar, J.M. and Schaltegger, U., 2002: The current state and future of accessory mineral research. *Chemical Geology, 191,* 3-24.

TABLE OF CONTENTS

REE mineral assemblages in igneous rocks: What can be learned from chemographic modelling?

Tom ANDERSEN

Department of Geosciences, University of Oslo, PO Box 1047 Blindern, N-0316 Oslo, Norway. tom.andersen@geo.uio.no

Chemographic modelling of multicomponent systems has been used with a certain success to establish the relative stability relationships of HFSE-bearing mineral assemblages in highly alkaline rocks (e.g. Andersen *et al.* 2010, 2012, Marks *et al.* 2011).The method is less easily applicable to REE-bearing mineral assemblages because of the complexity of REE distribution patterns and the lack of a dominant host mineral (such as zircon for Zr and ilmenite for Ti).

Using the methods described by Andersen *et al.* (2010), a tentative, semiquantitative grid of low-variance reactions in isobaric-isothermal log activity (or chemical potential) space for LREE (represented by Ce^{3+}) bearing minerals can be constructed. The system considered is $NaO_{0.5}$-$KO_{0.5}$-CaO-FeO-$FeO_{1.5}$-$CeO_{1.5}$-TiO_2-$AlO_{1.5}$-SiO_2-$HO_{0.5}$-$PO_{2.5}$-$FO_{-0.5}$, and alkali feldspar, plagioclase, biotite, magnetite, ilmenite, titanite, apatite, ±fluorite, ±quartz, ± nepheline and silicate melt are assumed to be present. The choice of components and non-REE-bearing phases allows rock compositions ranging from anorthosite through metaluminous granite and granite pegmatites to miaskitic nepheline syenite to be approximated. REE minerals in the model are allanite-(Ce), chevkinite-(Ce), perrierite-(Ce), britholite-(Ce) and monazite-(Ce). The grid gives a reasonable representation of the relative stability relationships of these REE minerals, and provides a hint on which compositional parameters may cause the stability of the different minerals.

The parameters having the strongest influence on the stability of the LREE minerals at constant temperature and pressure.are the activities of silica, water and the anorthite component (in melt and plagioclase). Allanite has a wide stability field at elevated a_{An}, which wedges out towards low a_{An} (i.e. towards more alkaline compositions). In the model system, monazite is stable at high a_{SiO2}, and britholite at low a_{SiO2} (compatible with its normal occurrence in silica-undersaturated rocks). Chevkinite and perrierite are stable at

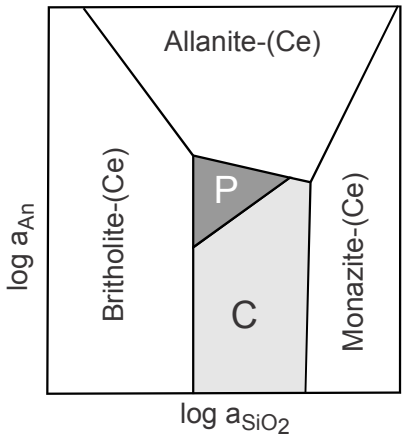

Fig. 1. Relative stability relationships of some LREE minerals coexisting with alkali feldspar, plagioclase, biotite, magnetite, ilmenite, titanite, apatite, fluorite and silicate melt projected to the *log* a_{SiO2}-*log* a_{An} plane. *C*: Chevkinite-(Ce), *P*: Perrierite-(Ce).

intermediate silica activity, perrierite at higher a_{An} than chevkinite, in agreement with its common association with mafic rocks (Fig. 1). Oxygen fugacity and fluorine activity have only a minor influence on the relative stability relationships, except that the monazite field contracts towards higher a_{SiO2} at elevated a_{HF}. On the other hand, elevated water activity causes the monazite field to expand towards lower a_{SiO2}, which will eventually cause the chevkinite and perrierite fields to disappear, perrierite being more sensitive to water than chevkinite.

The phase diagrams shown in Figs. 1 and 2 are extreme simplifications which aim to illustrate some general features of REE mineral stability. In nature, all of these minerals have variable compositions, which may be quite far removed from the ideal compositions used here. For the method to be applicable to real rocks, both mineral analyses from the rock of interest and detailed observations on coexisting mineral assemblages are needed.

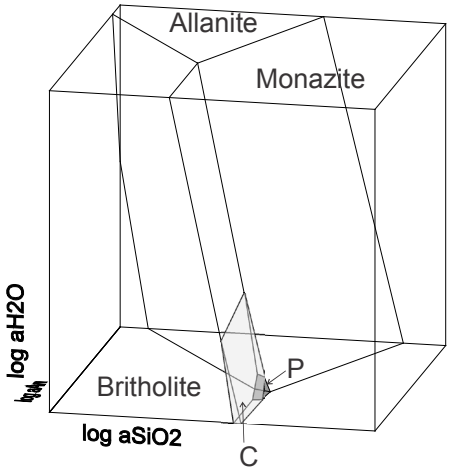

Fig. 2. A 3D rendering of stability relationships in $log\ a_{SiO2} - log\ a_{An} - log\ a_{H2O}$ space. *C*: Chevkinite-(Ce), *P*: Perrierite-(Ce).

References

Andersen, T., Erambert, M., Larsen, A. O., Selbekk, R. S., 2010: Petrology of Nepheline Syenite Pegmatites in the Oslo Rift, Norway: Zirconium Silicate Mineral Assemblages as Indicators of Alkalinity and Volatile Fugacity in Mildly Agpaitic Magma. *Journal of Petrology, 51*(11), 2303-2325.

Andersen, T., Elburg, M., Erambert, M., 2012: Petrology of combeite- and götzenite-bearing nephelinite at Nyiragongo, Virunga Volcanic Province in the East African Rift. *Lithos, 152*, 105-121.

Marks, M.A.W., Hettmann, K., Schilling, J., Frost, B. R., Markl, G., 2011: The mineralogical diversity of alkaline igneous rocks: Critical factors for the transition from miaskitic to agpaitic phase assemblages. *Journal of Petrology 52*(3*)*, 439-455.

Monazite in mixed magmas from the Strzegom Massif

Bogusław BAGIŃSKI[1], Justyna DOMAŃSKA-SIUDA [1], Ray MACDONALD[1]

[1]*University of Warsaw, Faculty of Geology, Institute of Geochemistry, Mineralogy and Petrology, al. Żwirki i Wigury 93, 02-089 Warszawa; e-mail b.baginski1@uw.edu.pl*

We report on monazites of unusually large size (up to 500 μm) which grew at the interface between intermediate and salic magmas (Turniak *et al.* 2014) their growth apparently being promoted by mixing between the magmas. The monazites also show detailed textural and compositional features related to hydrothermal activity in the host rocks. Our aim is to increase our understanding of the conditions under which monazite can crystallize and recrystallize in igneous rocks.

Within the area of an ordinary thin section located on the boundary between granodiorite/granite and a slightly darker enclave (granodiorite/tonalite), we have found up to 100 crystals of monazite (10 microns or bigger). Most of them are located within the rim zone of the enclaves. They show clear oscillatory zoning typical of magmatic origin. Compositional zoning is most prominent in Th content (which in some large crystals varies from 23.8% in the core to 2% Th in the rim). We relate the unusual growth of monazite crystals to the process of magma mixing, which is reflected in plagioclase crystals in the enclaves, showing distinct reversed and/or oscillatory zoning (An_{46} to An_{9}). Large euhedral or subhedral, patchily zoned, crystals up to 5 mm are sometimes present. There has clearly been movement of these large crystals between the two magmas. The process has been documented from many plutons (for example, reported megacryst movement between melts in the Karkonosze pluton, Słaby *et al.* 2007). The change of temperature and/or the composition of melt could be responsible for the resorption of many monazite crystals.

More than 15% of monazites show different alteration styles (Fig. 1 A-F). Three general kinds of alteration are dominant:

1) Monazite > Apatite (Fig. 1A) - type connected with deformation
2) Monazite > Apatite + Allanite (Fig. 1 C-F), similar to that reported by Broska and Siman (1998) and Dini et al. (2004)
3) Monazite > Apatite + Allanite + Xenotime + a REE phase (Fig. 1B shows the considerable mobilization of LREE)

References

Broska, I., and Siman, P., 1998: The breakdown of monazite in the West-Carpathian Veporic orthogneisses and Tatric granites. *Geologica Carpathica*, *49*, 161-167.

Dini, A., Rocchi, S., and Westerman, D.S,. 2004: Reaction microtextures of REE-Y-Th-U accessory minerals in the Monte Capanne pluton, Elba Island, Italy): a possible indicator of hybridization processes. *Lithos*, *78*, 101-118.

Słaby, E., Seltmann, R., Kober, B., Müller, A., Galbarczyk-Gasiorkowska, L. and Jefferies, T., 2007: *LREE* distribution patterns in zoned alkali feldspar megacrysts from the Karkonosze pluton, Bohemian Massif – implications for parental magma composition. *Mineralogical Magazine, 71*, 155-178.

Turniak, K., Mazur, S., Domańska-Siuda, J., Szuszkiewicz, A., 2014: SHRIMP U-Pb zircon dating for granitoids from the Strzegom - Sobótka Massif, SW Poland: Constraints on the initial time of Permo- Mesozoic lithosphere thinning beneath Central Europe. *Lithos (in press)*

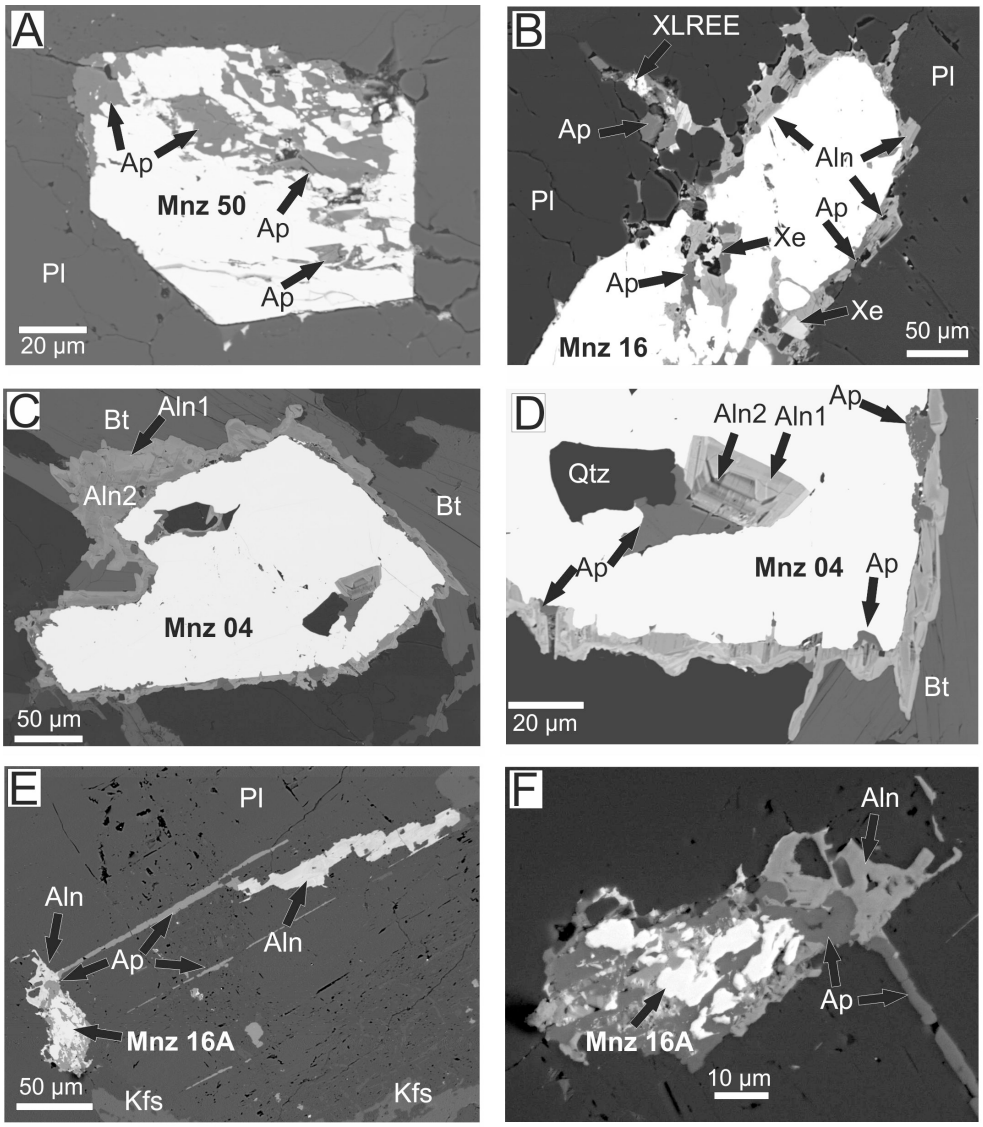

Fig. 1. Back-scattered electron images of different monazite alteration styles; Strzeblów granite, sample D125. (a) Euhedral (magmatic) monazite in plagioclase, patchily replaced by apatite along cracks. The cracks are ascribed to deformation along the major fault zone, located in the vicinity. (b) Euhedral (magmatic) monazite was cracked and deformed with replacement by allanite, apatite and xenotime. The crystal is rimmed by allanite and apatite (c.f. (b)). Above the monazite is a complex intergrowth of apatite, allanite and a LREE-rich allanite (light). The zone is ascribed to hydrothermal fluids migrating into the host quartz. (c) Euhedral (magmatic) monazite which was partially resorbed and rimmed by allanite ± apatite, the apatite occurring as isolated strips and patches in the allanite. The monazite crystal contains two quartz inclusions associated with replacive allanite and apatite. (d) Detail of inclusion in (c). Allanite type 1 shows oscillatory zoning, with overgrowths of allanite type 2. (e) Monazite (magmatic?) largely replaced by allanite and apatite. Apatite clearly connected to the monazite has formed along cleavage planes in the host plagioclase. The mid-grey elongated patch is allanite. (f) Detail from (e) to show the replacement texture in the monazite crystal.

REE, Y, Zr, and Nb mineralogy of the Neoproterozoic Robertson River igneous suite, northern Virginia, USA

Harvey E. BELKIN

U.S. Geological Survey, MS956, Reston, VA 20192 USA; hbelkin@usgs.gov

The Blue Ridge province is both a physiographic and geologic province in the Appalachian Mountains, eastern United States. Mostly tree covered, the Blue Ridge Mountains have average heights of 600 to 1200 m with a maximum of about 2000 m. In northern Virginia, the Blue Ridge province forms a basement massif with Mesoproterozoic Grenville-age (1.2-1.0 Ga) crystalline rock in its core and Late Neoproterozoic to Early Paleozoic cover rock on its flanks. The Blue Ridge province is allochthonous and has been thrust to the northwest over Paleozoic rocks of the Valley and Ridge province. Although earlier deformation events are recorded in the older igneous and metamorphic rocks, the Blue Ridge is a complex anticlinorium structure that experienced deformation and crustal shortening during the Paleozoic. In Virginia, the Blue Ridge separates the fossiliferous Paleozoic sedimentary sequence on the west from the metamorphic and igneous Piedmont province to the east.

The Robertson River igneous suite is the largest Neoproterozoic A-type granite body emplaced along the eastern Blue Ridge flank. Eight plutons constitute the elongate (110 km by ≤5 km) Robertson River batholith (Tollo and Lowe 1994). Uranium–lead isotopic analyses (TIMS) of zircons indicate emplacement in two magmatic pulses: about 735–722 and 706–702 Ma. (Tollo and Aleinikoff, 1996). Metaluminous magmas were emplaced during both pulses and form most of the batholith. Peralkaline magmas constitute the Amissville granite and Battle Mountain volcanic center and (Tollo 1994) that erupted unknown quantities of rhyolite during the final phase of Robertson River activity. The igneous body appears to be a multiply intruded large dike-shaped sheet emplaced episodically into basement during regional Rodinian crustal extension related to the opening of Iapetus. Eight formations can be distinguished divided between the two magmatic pulses (Tollo 1994). The second pulse of magmatism consists of the Hitt Mountain alkali feldspar syenite, Amissville alkali feldspar granite and the Battle Mountain complex. The Amissville and Battle Mountain rocks have exceptionally high trace-element contents; Zr ~1000 ppm, Nb ~200 ppm, and Σ Y, Sc, REE > 1000 ppm. Fluorite is abundant in the entire Robertson River suite and a plethora of accessory minerals (Tollo and Lowe 1994).

The current study aims to examine the primary and secondary mafic mineral assemblages (Na, Fe-rich amphibole, biotite, aegirine, and stilpnomelane) and to characterize the trace element mode of occurrence and metasomatic alteration sequence(s). This discussion focuses on the trace element accessory mineralogy with emphasis on rare-earth element (REE), Y, Zr, and Nb-bearing phases in the peralkaline portion of the Robertson River suite. Electron microprobe analysis coupled with SEM imaging were the analytical tools.

Zircon is the only Zr-phase observed and ranges in habit from euhedral, millimeter long crystals to hydrothermal amoeboid, commonly altered masses. HfO_2 content ranges from 0.49 to 3.14 wt% and the mean ΣREE, Y is 1.3 wt%; the Zr/Hf ratio (w/w) varies from 17 to 82.

The major REE-bearing phases are fluorocarbonate, a chevkinite group mineral, allanite, gadolinite, and a variety of Nb phases. Bastnäsite-(Ce) is the major fluorocarbonate with minor parisite-(Ce), and synchysite-(Ce).

The chevkinite group minerals in the peralkaline rocks average 11.50 wt% FeO and 2.60 wt% CaO, (SrO is essentially nil) and are classified as chevkinite-(Ce) by Macdonald and Belkin (2002). Alteration was commonly observed and leads to a reduction in LREE, but not HREE, an increase in Nb, Ti, and Pb and a decrease in Si with accompanying hydration.

Allanite-(Ce) occurs in a wide variety of habits from subhedral crystals to amoeboidal masses and averages 25 wt% ΣREE. Gadolinite-(Y) occurs as euhedral to subhedral crystals, sometimes zoned, and averages 52 wt% ΣREE, Y.

The Nb-bearing phases occur in a wide variety of chemistry, habits, and typically show alteration or multiple generations. Using the canonical classification of Ercit (2005), two major groups, aeschynite-euxenite and pyrochlore were identified. The aeschynite group has two groups, one with REE>Y and the other Y>REE; euxenite was a minor phase. Total REE for all Nb-bearing phases ranges from 9 to 30 wt% with the dominant element Nd, Sm or Gd. Columbite-(Fe) was observed, but contained minor REE. Nb/Ta (w/w) for the aeschynite-euxenite group ranges from 4 to 79, whereas the pyrochlore group which may, in part, be an alteration product has values from 19 to >7000 where Ta is at or below microprobe detection limit.

Many phases show alteration, or deposition by late-stage fluids. The mafic assemblage, especially in the peralkaline rocks, is dominated by aegirine, riebeckite, and stilpnomelane; fluorite is ubiquitous. The mineralogy and petrography suggest Na-, Fe-, and F-rich fluids carrying REE, Y, Nb, and Zr were late-stage and moved through the rock during the early cooling process.

Questions not addressed here, but currently being pursued, involve the relationship of the Robertson River complex to similar rocks exposed further south along the Blue Ridge and the melting process and environment giving rise to these trace-element enriched rocks.

References

Ercit, T.S., 2005: Identification and alteration trends of granitic-pegmatite-hosted (Y,REE,U, Th)-(Nb,Ta,Ti) oxide minerals: A statistical approach. *The Canadian Mineralogist, 43*, 1291-1303.

Macdonald, R. and Belkin H.E., 2002: Compositional variation in minerals of the chevkinite group. *Mineralogical Magazine, 66*, 1075-1098.

Tollo, R.P., 1994: Definition and nomenclature of the Robertson River Igneous Suite, Blue Ridge Province, Virginia. Stratigraphic Notes, 1992. *U.S. Geological Survey Bulletin 2060*, 19-24.

Tollo, R.P., Aleinikoff, J.N., 1996: Petrology and U–Pb geochronology of the Robertson River Igneous Suite, Blue Ridge province, Virginia: evidence for multistage magmatism associated with an early episode of Laurentian rifting. *American Journal of Science, 296*, 1045-1090.

Tollo, R.P., Lowe, T.K., 1994: Geologic map of the Robertson River Igneous Suite, Blue Ridge Province, Virginia. U.S. Geological Survey Miscellaneous Field Studies Map MF-2229, scale 1:100000, 15 p.

Apatite stability in examples from low- to high-metamorphic conditions

Igor BROSKA[1], Pavel UHER[3], Erling KROGH RAVNA[2], Marian JANÁK[1], Kare KULLERUD[2], Jarmila LUPTÁKOVÁ[1], Peter BAČÍK[2], Peter VOJTKO[1], Ján MADARÁS[1]

[1]*Geological Institute, SAS, Dúbravská cesta 9, 840 05 Bratislava, Slovakia; igor.broska@savba.sk*
[2]*Department of Geology, University of Tromsø, N-9037 Tromsø, Norway*
[3]*Comenius University in Bratislava, Faculty of Natural Sciences, Mlynská Dolina 1, Bratislava*

Introduction

Being widespread minerals in crustal rocks, accessory apatite is an important source of information on the evolution of its parental magmas, and on postmagmatic hydrothermal and metamorphic processes altering the composition of the rocks, recently including also age information. In polymetamorphic terrains such as the Western Carpathians, the generally accessory mineral assemblage may experience several metamorphic events which are used in the reconstruction of geological events on the larger scale (Broska and Petrík 2014). This contribution will be a presentation of examples of apatite alteration in (1) low-grade metamorphosed and (2) medium grade metamorphosed granitic rocks from the Western Carpathians (3) and HP/UHP conditions mostly as a result of a fluid-mediated regime from the Scandinavian Caledonides. In addition the geological implication of a xenotime-Y-rich - apatite - epidote system will be shown using an example from the Tribeč Mts. (Western Carpathians).

Apatite stability under various conditions

(1) Alteration of apatite in biotite granodiorite of the Malá Fatra Mts. (Slovakia) shows the penetration effect of fluids through apatite nanochannels and the metasomatic formation of monazite due to REE mobility. In this way monazite metasomatised the apatite along its c-axis. Altered apatite was formerly precipitated along with mantled allanite-(Ce) during Lower Carboniferous intrusion as a primary phase; monazite precipitated as a product of Alpine overprinting. Monazite CHIME dating in the range Upper Permian to Cretaceous indicates an open system and therefore the age of monazite precipitation is imprecisely determined, although a Permian as well as Jurassic age in such circumstances could be expected.

(2) Newly-formed apatite is commonly observed among the products of monazite-(Ce) and xenotime-(Y) breakdown during medium-grade metamorphism where a suitable fluid composition occurs. Apatite is a transitional phase between former monazite in the core and allanite-(Ce) or epidote in the rim of coronas (Finger *et al.* 1998). The origin of small secondary phases (typically Th-rich) around the breaking-down monazite-(Ce) and xenotime-(Y) when apatite – allanite – REE-epidote coronas were being formed has not been clarified and the phases have not been precisely identified. In specific cases, during a change of the fluid regime, REE carbonates [e.g. hydroxylbastnäsite-(Ce)], were also formed by the CO_2-rich fluids after the breakdown of monazite and apatite and epidote formation. This process, first described by Bartek Budzyń in Poland, is documented also in the Veporic basement orthognesisses (Ondrejka *et al.* 2012). Recently the origin of fluorapatite and epidote, or allanite-(Ce) from monazite-(Ce) resulting from high Ca-activity in the fluids was confirmed by experiments showing the chemistry of the system (Budzyń *et al.* 2011). It was demonstrated

that the decrease of Ca and increase of Na concentrations in fluids lower the solubility of monazite, promoting direct allanite-(Ce) formation without apatite accompanied by numerous secondary monazites in coronas. On the other hand, high concentrations of K in the fluids promote the direct formation of apatite enriched in the britholite component (Budzyń *et al.* 2011). The alteration of apatite to britholite (substitution (Y+REE) + Si = Ca + P) was described in post-orogenic A-type granites with high K contents, britholite forming at the expense of primary magmatic fluorapatite due to late-magmatic fluids (Uher and Ondrejka 2008).

(3) The behaviour of apatite, monazite and xenotime-(Y) in high- and ultrahigh-pressure conditions (UHP) is very specific and at present is being studied at several places around the world. The formation of oriented tiny trellis inclusions of monazite in apatite during decompression from a UHP environment indicates that apatite in high-pressure conditions is able to incorporate greater amounts of the REE which during decompression are unmixed to newly-formed monazite (Krenn *et al.* 2009). Harlov and Förster (2002) described a similar association of REE-poor apatite + monazite from an original REE-rich apatite. The retrogression regime following the progressive metamorphic phase may trigger not only the exsolution processes resulting in the precipitation of new minerals within the apatite crystals (e.g. formation of monazite) but also wide metasomatic precipitation as a product of fluid–aided activities. An example of the formation of inclusions in apatite is the presence of long tiny pyrrhotite rods found in fluorapatite from silicate-bearing carbonate rocks associated with UHP eclogites in the Tromsø Nappe from Scandinavian Caledonides (Broska *et al.* in press). Relaxation of the fluorapatite structure during retrogression/decompression plays a significant role in the a-axis direction, enhancing the formation of new phases. The a/c ratio is negatively correlated to pressure and compression is probably a result of the greater compressibility of nanochannels in the fluorapatite. The fluid-mediated regime implies rapid precipitation of different phases in the apatite nanochannels during retrogression of HP/UHP rocks.

Geological implication of phosphate stability

The geological implication of phosphate stability in igneous rocks can be demonstrated from the Tribeč Mts. which contain weakly Alpine overprinted Variscan I- and S--type granites distributed mostly in the valleys. According to Zr- thermometry and Al-in hornblende geobarometry these mostly I-type granitoids were formed at a temperature of 800 °C and pressure ca 400 MPa. On the other hand, the mountain ridge in the Tribeč Mts. is composed of deformed mylonitised granitoids with locally abundant minute altered monazite-(Ce) and xenotime-(Y) to apatite and epidote (allanite) coronas. Experimental work pointed to minimum pressure conditions for such xenotime-(Y) breakdown as 800 MPa (Budzyń personal communication) forming a metamorphic contrast of the deeper undeformed granite massif and the upper mylonitised part of granites. Such conditions indicate the overriding of two different granitic blocks. Upper granitoids superimposed by Alpine amphibolite facies known from the Veporic unit in a position above the undeformed Tatric granite massif implies overlapping. In other words, xenotime-(Y) breakdown observed in the mylonitised granites from the Tribeč mountain ridge indicates the presence of the Veporic nappe system on the Tatric unit, which leads to a new understanding of the geological structure of the Tribeč Mts.

References

Broska I., Petrík I., 2014: Accessory phases in the genesis of the igneous rocks. In: S. Kumar and R. N. Singh (eds.), Modelling of Magmatic and Allied Processes. *Society of Earth Scientists Series*, 109-149.

Broska I., Ravna E.J., Vojtko P., Janák M., Konečný P., Pentrák M., Bačík P., Luptáková J., Kullerd K., Oriented inclusions in apatite in a post-UHP fluid-mediated regime (Tromsø nappe, Norway). *European. Journal of Mineralalogy (in press).*

Budzyń B., Harlov D., Williams M. L., Jercinovic M. J., 2011: Experimental determination of stability relations between monazite, fluorapatite, allanite, and REE-epidote as a function of pressure, temperature, and fluid composition. *American Minereralogist, 96*, 1547-1567.

Finger, F., Broska, I., Roberts, M.P., Schermaier, A., 1998: Replacement of primary monazite by apatite–allanite–epidote coronas in an amphibolite facies granite gneiss from the eastern Alps. *American Minereralogist 83*, 248-258.

Krenn E., Janák M., Finger F., Broska I., Konečný P., 2009: Two types of metamorphic monazite with contrasting La/Nd, Th, and Y signatures in an ultrahigh-pressure metapelite from the Pohorje Mountains, Slovenia: Indications for pressure-dependent REE exchange between apatite and monazite? *American Mineralogist, 94*, 5-6, 801-815.

Ondrejka M., Uher P., Putiš M., Broska I., Bačík P., Konečný P., Schmiedt I., 2012: Two-stage breakdown of monazite by post-magmatic and metamorphic fluids: An example from the Veporic orthogneiss, Western Carpathians, Slovakia. *Lithos 142-143*, 245-255.

Uher P., Ondrejka M., 2008: Britolit-(Y): neskoromagmatický akcesorický minerál Y-REE z granitu A-typu v Stupnom pri Považskej Bystrici, Pieninské bradlové pásmo (severozápadné Slovensko). *Bulletin Mineralogicko-Petrologického Oddělení Národního Muzea (Praha) 16/2*, 224-229.

Crystal chemistry of layered titanium silicates

Fernando CAMARA[1], Elena SOKOLOVA[2]

[1]*Dipartimento di Scienze della Terra, Università di Torino, Via Valperga Caluso 35, 10125, Torino, Italy; e-mail: fernando.camaraartigas@unito.it*
[2]*Department of Geological Sciences, University of Manitoba, Winnipeg, Manitoba R3T 2N2, Canada; e-mail: Elena.Sokolova@umanitoba.ca*

Layered titanium silicates are common accessory phases in peralkaline rocks. Their accessory character can, however, have economic importance as they may host significant quantities of *REE* elements. Understanding their crystal-chemistry can shed light on the petrologic and geochemical evolution of the host rocks. Complex structure topologies in these minerals challenge researchers to reach correct crystal-chemical formulas, even with a sound knowledge of how to handle mineral chemistry in more general and simple phases. This difficulty adds to that provided by the complex chemistry that makes complete chemical analysis demanding. In particular when *REE* are involved it is necessary to take particular care over line overlaps that must be properly corrected and in avoiding background interferences. The same applies to the ubiquitous presence of Ba and Ti. A proper description of mineral structures helps us to attain the correct normalization schemes and to understand the feasibility and limits to chemical coupled substitutions.

A brief description of structural hierarchies in layered titanium silicates will be provided along with consideration of the crystal-chemical variations in rinkite $Na_2Ca_4REETi(Si_2O_7)_2OF_3$, nacareniobsite-(Ce) $Na_3Ca_3REENb(Si_2O_7)_2OF_3$ and mosandrite $[(H_2O)_2Ca_{0.5}\square_{0.5}]Ca_3REETi(Si_2O_7)_2(OH)_2(H_2O)_2$, and Group-I TS-block minerals (Sokolova 2006, Sokolova and Cámara 2013).

References

Sokolova, E., 2006: From structure topology to chemical composition. I. Structural hierarchy and stereochemistry in titanium disilicate minerals. *Canadian Mineralogist, 44*, 1273-1330.

Sokolova, E. and Cámara, F., 2013: From structure topology to chemical composition. XVI. New developments in the crystal chemistry and prediction of new structures topologies for titanium disilicates minerals with the TS-block. *Canadian Mineralogist, 51*, 861-891.

Experimental high-grade alteration of zircon using alkali-bearing and Ca-bearing solutions: Nature and experiment

Daniel E. HARLOV[1], Robert ANCZKIEWICZ[2], Alexander LEWERENTZ[3], Daniel J. DUNKLEY[4], and Anders SCHERSTEN[3]

[1]*GeoForschungsZentrum Telegrafenberg, D-14473 Potsdam, Germany; dharlov@gfz-potsdam.de*
[2]*Institute of Geological Sciences, Polish Academy of Sciences, 31-002 Krakow, Poland; ndanczki@cyf-kr.edu.pl*
[3]*Department of Earth Sciences, Lund University, 22362 Lund, Sweden,*
[4]*Applied Geology, Western Australian School of Mines, Curtin University, 6845 Perth, Australia*

In nature zircon is one of the principal accessory minerals used for the dating of geologic processes. As a consequence, the stability of zircon in the presence of various possible metamorphic and igneous fluids under a range of P-T conditions and its subsequent alteration with respect to some of these fluids has begun to be explored experimentally as well as speculated upon in a series of natural studies of metasomatized zircons (see review in Geisler *et al.* 2007). The natural alteration of zircon takes place either via dissolution coupled with overgrowth or via fluid-aided coupled dissolution-reprecipitation (Putnis 2009). This process results in the zircon being partially or totally replaced by new compositionally re-equilibrated zircon or a new mineral phase or both.

In this study, fragments (50 to 200 microns) from a large, inclusion-free, clear, light brown, relatively non-metamict euhedral zircon collected from a nepheline syenite pegmatite (Seiland magmatic province, northern Norway) were experimentally reacted in 20 mg batches with a series of alkali-and Ca-bearing fluids plus a Th + Si source (5 mg ThO_2 + $ThSiO_2$ + SiO_2) in sealed Pt capsules at 900 °C and 1000 MPa for 6 to 11 days in the piston cylinder press using a CaF_2 setup with cylindrical graphite oven. Fluids included 5 mg 2 N NaOH, 5 mg 2 N KOH, 10 mg $Na_2Si_2O_5$ + 5 mg H_2O, 1 mg NaF + 5 mg H_2O, and 1 – 5 mg $Ca(OH)_2$ + 5 mg H_2O. In each experiment, the fluid reacted with the zircon. This reaction took the form of partial replacement of the zircon with compositionally altered zircon via coupled dissolution-reprecipitation plus varying amounts of overgrowth. The reacted zircon is characterized by a sharp compositional boundary between the altered and original zircon as well as, in some cases, by a micro-porosity and/or inclusions of ZrO_2 or $ThSiO_4$. LA-ICPMS and SIMS analyses of the replaced zircon indicates that it is strongly enriched in Th, heavily depleted in U, and heavily to moderately depleted in (Y+REE). If YPO_4 replaces (Th + Si) in the system, the altered zircon is enriched in YPO_4 and heavily depleted in Th and U. TEM of FIB foils taken across the reaction front indicate no change in the crystallography of the altered zircon compared to the unaltered zircon. In all experiments radiogenic ^{206}Pb (3 to 5 ppm in the unaltered zircon) is strongly depleted in the altered zircon to below the SIMS and LA-ICPMS detection limits. Hafnium concentrations in the altered zircon retain the same value as in the original zircon. The results from these experiments indicate that zircon can be compositionally altered via alkali- and Ca-bearing fluids via coupled dissolution-reprecipitation processes under high-grade conditions and that its internal geochronometer can be reset due to the massive loss of radiogenic Pb.

In experiments where the zircon was metasomatized in $Ca(OH)_2$ + H_2O, inclusions of baddeleyite (ZrO_2) are seen outlining the reaction front between the altered and unaltered zircon. The baddeleyite-zircon textures from these experiments replicate similar, highly-localized zircon-baddeleyite textures seen in albitized, 2.9 to 2.7 Ga, amphibolite- and granulite-facies granitoid rocks from SW Greenland (Windley and Garde 2009). Here Ca was released into the fluid during the albitization of plagioclase. Baddeleyite should not be stable in the presence of SiO_2 (present in both the experiments and in the granitoid

rocks) but rather react with SiO_2 to form zircon. However, if sufficient Ca is present in the fluid, it appears to complex with the SiO_2 as $CaSiO_3$ thereby lowering the SiO_2 activity such that baddeleyite is stable with co-existing zircon and quartz. The experiments also demonstrated that, with sufficiently high enough concentrations of SiO_2 in the fluid, not all of the SiO_2 will complex with Ca, allowing for the activity of SiO_2 to remain at 1. In this case baddeleyite did not form in or with the altered zircon

References

Geisler, T., Schaltegger, U., Tomaschek, F., 2007: Re-equilibration of zircon in aqueous fluids and melts. *Elements 3,* 43-50.

Putnis A., 2009: Mineral Replacement Reactions. In: Oelkers E.H., Shott J.. (Eds.), Minerals, Inclusions and Volcanic Processes. *Reviews in Mineralogy and Geochemistry, 70*, 87-124.

Windley, B.F, Garde A.A., 2009: Arc-generated blocks with crustal sections in the North Atlantic craton of West Greenland: Crustal growth in the Archean with modern analogues. *Earth-Science Reviews, 93*, 1-30.

Classification diagram for REE-bearing members of the epidote group based on crystallochemical data

Pavel M. KARTASHOV

Institute Geology of Ore Deposits (IGEM RAS), Moscow, e-mail: pmk@igem.ru

More than 200 years have passed since the first description of epidote by Haui in 1801. Since then, 29 members approved by the IMA have joined the epidote group. Minerals of the group have the general formula $A_2M_3[Si_2O_7][SiO_4]X_2$ where A=Ca, REE + Y, Sr, Mn, Pb, M=Al, Fe, Mn, Mg, V, Cr and X=O, OH and F. Minor and very limited quantities of Th and U are able to enter the A site and Ti and Sc can go into the M site. Besides that, some Al is also able to replace Si in the tetrahedra $[SiO_4]$. All members of the group are monoclinic $P2_1/m$. Zoisite is the orthorhombic polymorph of clinozoisite and is not considered a member of the epidote group.

Three distinct subgroups are recognised within the group: a subgroup poor in REE epidote and the REE-rich subgroups allanite and dollaseite. Minerals of the epidote subgroup are connected with the allanite row by the heterovalent isomorphic substitution $Ca^{2+} + Me^{3+} = REE^{3+} + Me^{2+}$ (I) where Me^{3+} = Al, Fe, Mn, V and Me^{2+}= Fe, Mn, Mg. Thus, in minerals of the epidote subgroup, ΣREE and consequently Me^{2+} in octahedral sites always are ≤0.5 f.u. In turn, minerals of the allanite subgroup are connected with the dollaseite subgroup by replacement *via* the scheme $Me^{3+} + O^{2-} = Me^{2+} + (F,OH)^-$ (II). According to this scheme, the sum of Me^{2+} in the octahedral positions of allanite subgroup minerals is located in interval 0.5≤n≤1.5 f.u. Whilst for dollaseite row minerals it is 1.5≤n≤2 f.e. and ΣREE is limited to 0.5≤n≤1 f.u. in both cases.

Before 2002, the chemical approach had predominated during the subdivision of new mineral species in the epidote group. In other words, new mineral species were divided on the basis of the predominance of some chemical elements in some formula positions A or M. For example, in 1995 when we began to work with the mineral ferriallanite, we understood that allanite minerals had Fe^{3+} contents ≤1 f.u.. Consequently only minerals with ≤1 f.u. of Al were considered by us to be ferriallanite. After publication of Ercit's article (Erict 2002), the crystallochemical approach prevailed. As a result, changes in nomenclature were published in 2006 (Armburster *et al.* 2006). Now seven nonequivalent positions are recognised in the epidote formula **A1**A2M1M2**M3**$[Si_2O_7][SiO_4]$X1X2 where A1 and M3 are key cation sites. The population of these key sites is essential for the determination of the root name of epidote group species. In the epidote subgroup, the A1 site is invariably populated by Ca, and according to their population of M3 site root names ***clinozoisite*** (Al), ***epidote*** (Fe^{3+}), ***piemontite*** (Mn^{3+}) and ***mukhinite*** (V^{3+}) were accepted. Similarly in the allanite subgroup ***allanite*** (A1-Ca, M3-Fe^{2+}) and ***androsite*** (A1-Mn^{2+}, M3-Mn^{2+}) root names were divided. Dollaseite is the rarest in nature and the subgroup is represented by only two species with their own root names – ***dollaseite*** (A1-Ca, M3-Mg^{2+}) and ***khristovite*** (A1-Ca, M3-Mn^{2+}). The predominance of a new element in any of these cation positions would allow us to discover a new mineral species within the group.

After 2006 eight new epidote group members were discovered, six of them belonging to the allanite subgroup: uedaite-(Ce) (IMA2006-022), allanite-(Nd) (IMA2010-060), ferriallanite-(La) (IMA2010-066), vanadoallanite-(La) (IMA2012-095), ferriakasakaite-(La) (IMA2013-126) and ferriandrosite-(La) (IMA2013-127). As we can see, two new root names were accepted – ***uedaite*** (A1-Mn^{2+}, M3-Fe^{2+}) and ***akasakaite*** (A1-Ca, M3-Mn^{2+}). One new mineral piemontite-(Pb) (IMA2011-87) was added to the epidote subgroup. Besides that, the discovery of askagenite-(Nd) (IMA2009-073) generated

a new subgroup in the epidote group. The mineral with composition $Mn^{2+}NdAlAlFe^{3+}[Si_2O_7][SiO_4]OO$ is related to epidote by the isomorphic substitution $Ca^{2+} + OH^- = REE^{3+} + O^{2-}$ (III) and to allanite by the substitution $Fe^{2+} + OH^- = Fe^{3+} + O^{2-}$ (IV).

A fundamental fault of such a crystallochemical approch is the necessity of determining the crystalline structure of the mineral for attribution to one or another mineral species. At the moment, the number of analyses of epidote group minerals exceeds some thousands, whilst structures have been solved for only 30-35 of them. Often, therefore, uncertainties in a simple determination of epidote group minerals arise (Ericit, 2002). We have made an attempt to find a way out of such a situation by plotting the contents (in f.u.) of the octahedral cations M on the triangular diagram Me^{3+}-Al_{VI}-Me^{2+} where Me^{3+}=Fe, Mn, V, Cr or their sum and Me^{2+}=Fe,Mn, Mg. The diagram (Fig.1) allows us to represent graphically complex isomorphous transitions between minerals of the allanite and dollaseite subgroups and REE-bearing members of epidote subgroup, and allocate any particular composition to the correct mineral species. But the diagram is inapplicable for minerals of the askagenite subgroup.

The proposed diagram is based on thefollowing principles:

1. Octahedral positions M are unequal in their volume — M3>M1>M2. Larger cations preferentially occupy the larger polyhedra. From this it follows that Me^{2+} firstlyenter positions M1, then M3 and never occupy M2 sites. In accordance with this, Al^{3+} preferentially occupies position M2, after that M1 and is able to enter into the M3 site. Ions of Me^{3+} are able in turn to occupy positions M3 and M1, and also able in some cases to enter position M2, if it is not completely occupied by Al.
2. Divalent metals Me^{2+} are for simplicity considered as a single component — the sum Me^{2+} = Fe,Mn, Mg. The predominant component is used for classification (for example $Fe^{2+}_{0.45}Mg_{0.12}Mn^{2+}_{0.08}=Me^{2+}_{0.65}$ or $Fe^{2+}_{0.65}$). The same simplification should be used in the general case and for trivalent metals Me^{3+}=Fe, Mn, V, Cr (for example in the case $Fe^{3+}_{0.52}Cr^{3+}_{0.08}V^{3+}_{0.01}=Me^{3+}_{0.61}$ or $Fe^{3+}_{0.61}$). This is useful and has sense in cases of the simultaneous presence of two or more individual Me^{2+} or Me^{3+}in quantities significant for the division of mineral species (~25-33 f.u.); these are rare in nature.
3. The diagram should be divided into the compositional fields of nine end members (three components Me^{2+}, Me^{3+} and Al_{VI} are combined in three positions with the exclusion of the impossible combination $Me^{2+}Me^{2+}Me^{2+}$).
4. The boundaries of the compositional fields were drawn along points, coordinates of which contain uncertainties in at least one of three crystallochemical positions. For example, the point of composition $Me^{3+}_{1.5}Fe^{3+}_{0.75}Al_{0.75}$= $(Me^{2+}_{0.5}Fe^{3+}_{0.5})(Al_{0.75}Fe^{3+}_{0.25})(Me^{2+}_{1.0})$ is located on the boundary between fields $Me^{2+}AlMe^{2+}$ and $Fe^{3+}AlMe^{2+}$. All boundaries of the diagram were calculated by the numerical method.

On Fig. 1 is shown the diagram Fe^{3+}-Al_{VI}-Me^{2+} because it corresponds with the most naturally abundant compositions of the epidote group minerals. If necessary, Fe^{3+} can be simply replaced by any Me^{3+} (e.g. Mn^{3+} or V^{3+}). In Fig. 2 and Fig. 3 are given examples of the classification of epidote group minerals from two alkaline granite pegmatites from Ulyn Khuren Mt in Mongolia and metasomatic rocks of Eorae Mt in Southern Korea. Natural mineral species with the compositions $CaCeFe^{3+}Fe^{3+}Fe^{3+}[Si_2O_7][SiO_4]O(OH)$, $CaCeFe^{2+}AlFe^{2+}[Si_2O_7][SiO_4](OH)(OH)$ and $CaCaFe^{3+}AlFe^{3+}[Si_2O_7][SiO_4]O(OH)$ were detected by us as result of using of this diagram.

Reference

Ercit T.S., 2002: The mess that is “allanite”. *Canadian Mineralogist, 40*, 1411-1419.

Armbruster T., Bonazzi P., Akasaka M., Bermanec V., Chopin C., Gieré R., Heuss-Assbichler S., Liebscher A., Menchetti S., Pan Y., Pasero M., 2006: Recommended nomenclature of epidote-group minerals. *European Journal of Mineralogy, 18*, 551-567.

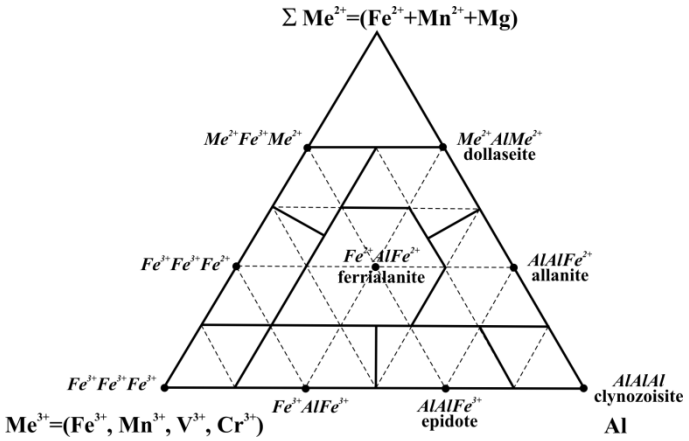

Fig. 1. Classification diagram for epidote group minerals in the system Fe^{3+}-Al_{VI}-Me^{2+}. Dots shows end members compositions.

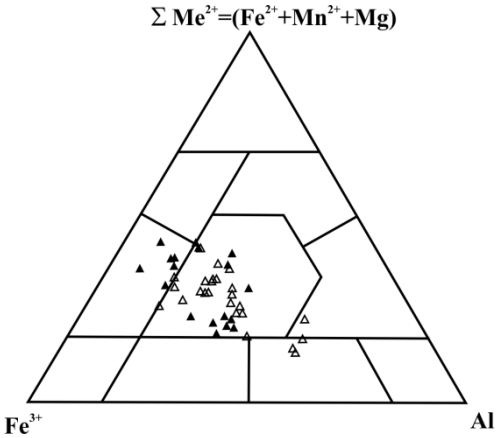

Fig. 2. Distribution and evolution of compositions of REE-bearing epidote group members in two alkaline granite pegmatites of Ulyn Khuren Mt (Mongolia). Closed triangles – Neprimetnyi pegmatite, open triangles – pseudomorphosed pegmatite.

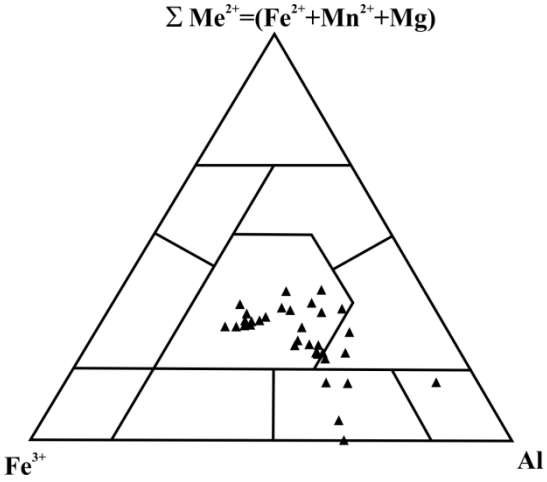

Fig. 3. Distribution and evolution of compositions of REE-bearing epidote group members in metasomatic rocks of Eorae Mt (S. Korea). There is a limited compositional field of ferriallanite from hematite associations in skarnoids and a continuous compositional trend from ferriallanite to epidote in magnetite associations in hornfels

Textural and compositional alterations in accessory zircon and monazite induced by F-bearing fluids.

Katarzyna LISOWIEC[1], Bartosz BUDZYŃ[2], Ewa SŁABY[1], Axel D. RENNO[3], Jens GÖTZE[4]

[1]*Institute of Geological Sciences, PASc, Research Centre in Warsaw, Twarda 51/55, 00-818, Warsaw, Poland; klisowiec@twarda.pan.pl, e.slaby@twarda.pan.pl*
[2]*Institute of Geological Sciences, PASc, Research Centre in Kraków, Senacka 1, 31-002, Kraków, Poland; ndbudzyn@cyf-kr.edu.pl*
[3]*Helmholtz-Zentrum Dresden-Rossendorf, Bautzner Landstraße 400, 01314 Dresden, Germany; a.renno@hzdr.de*
[4]*Institute of Mineralogy, TU Bergakademie Freiberg, Brennhausgasse 14, D-09596 Freiberg, Germany; jens.goetze@mineral.tu-freiberg.de*

Introduction

Accessory minerals are important targets in providing detailed records of granite petrogenesis, including melt sources, and magmatic and post-magmatic evolution (e.g. Uher *et al.* 2009). The chemical composition of accessory minerals can be used as a tool in recognizing even subtle changes and subsequent chemical modifications in the whole magmatic and post-magmatic environment. Some of them, particularly zircon, monazite, xenotime and apatite, are the main hosts of rare earth elements (REE) and actinides, and control the abundances of these elements in igneous systems, e.g. through their saturation and fractionation (Hoskin *et al.* 2000, Wark and Miller 1993, Evans and Hanson 1993 Dahlquist 2001). In this work, zircon and monazite (and to a lesser extent other Th-rich accessory minerals) are used to recognize and characterize post-magmatic alteration induced by possibly F-bearing fluids, recorded in both the textures and chemistry of these minerals.

Geological background

The granitoid pluton of Stolpen is located in the Lusatian Granodiorite Complex at the NE margin of the Bohemian Massif. It formed during the last stages of the Variscan orogenesis. The granite has a peraluminous character and crystallized from a crustal magma (Hammer *et al.* 1999), possibly enriched in mantle-derived fluids (Lisowiec *et al.* 2013, Lisowiec *et al.* 2014). It is accompanied by several dykes ranging from rhyolitic to andesitic. The granite samples for this study were taken from a marginal part of the batholith and include one medium-grained granite and fine-grained aplite. Additionally, a rhyolitic dyke located NW of the pluton was sampled.

Results and discussion

Zircon from the Stolpen granite shows magmatic oscillatory zoning overprinted by alteration textures such as discordant, convolute and patchy zoning as well as dissolution textures (Fig.1A). Their formation is explained by fluid interaction which can be divided into two stages separated by a strong dissolution event. The first stage involved the formation of Y-, P-, Th- and U-rich rims whilst during the second stage purification of these rims occurred. Elements released during this stage formed secondary minerals such as xenotime, monazite and thorite/huttonite. Grains from more aplitic parts of the granite demonstrate even stronger spongy-like textures which suggests more aggressive fluids (Fig.1B). Zircon from the rhyolite shows similar textures however the oscillatory zoning typical of magmatic crystallization occurs very rarely (Fig.1C). Domains indicating fluid-interaction are enriched in elements such as U, Th, P, Y, Ca and Fe. Numerous xenotime and cheralite inclusions can be found.

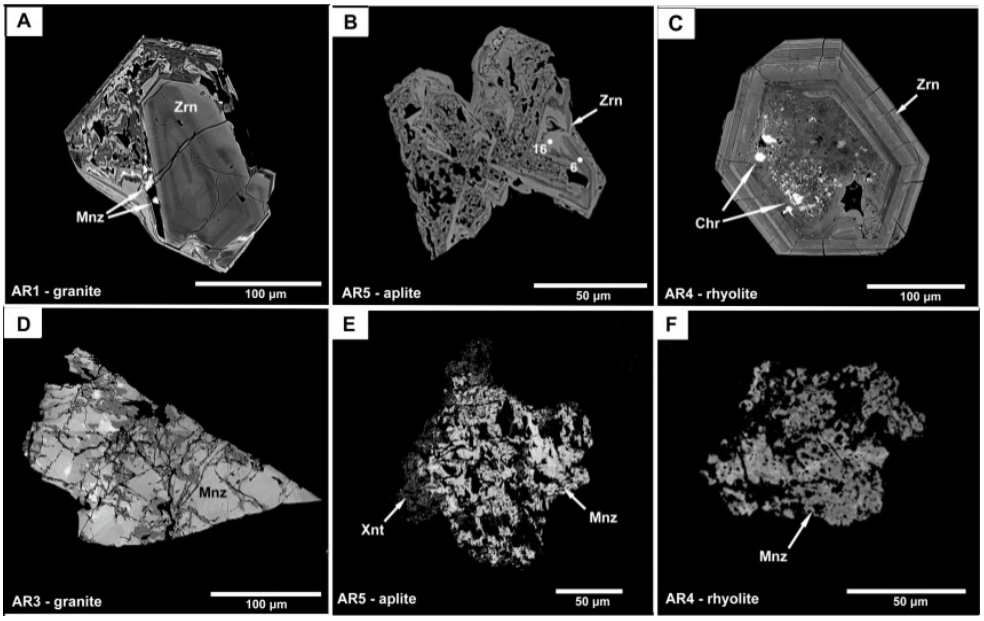

Fig.1. BSE images of zircon (A to C) and monazite (D to F) grains, showing various irregular and dissolution textures; *AR1 – granite* – sample name; mnz – monazite, zrn – zircon, chr – cheralite, xnt – xenotime

Monazite is a quite abundant accessory mineral in the granite and shows mostly heterogeneous textures including patchy and irregular zoning (Fig.1D). The chemical composition, especially the Ca- and Si- enrichment, suggests huttonite and cheralite substitutions. The patchy zoning probably resulted from the compositional alteration driven by the fluid-mediated coupled dissolution-reprecipitation process (e.g. Harlov *et al.* 2005). BSE-dark patches are depleted in Th, U and Pb which were selectively removed during the fluid-interaction. Monazite from the aplite exhibits mostly spongy textures resulting from strong dissolution (Fig.1E). Monazite from the rhyolite demonstrates similar textures resulting from intensive fluid-infiltration and dissolution (Fig.1F). It is depleted in Th which was incorporated into the cheralite end-member of the monazite-cheralite solid solution. A post-magmatic origin of the monazite grains in rhyolite is also indicated by a high PbO content.

Conclusions

Both zircon and monazite from the Stolpen granite and related rhyolitic dyke show signs of fluid-interaction such as irregular, patchy zoning, dissolution, spongy-like textures and modification of the chemical composition. The presence of fluorite in the granite suggests high F-activity in the fluid which is an important factor facilitating the dissolution of the minerals and element transport (Budzyń *et al.* 2011, Hecht *et al.* 1999). From the chemical alteration of the monazite and zircon grains from the granite we can assume that the fluids were enriched in Y, P, Th and U. In the rhyolite the fluids had a different character and were probably enriched in Ca, Si, Y and P. Their aggressive nature is supported by the strong dissolution of the minerals reflected in their porous texture.

The chemical composition of the altered domains and presence of other secondary accessory minerals such as fluorite, Nb-minerals, Y-rich minerals is difficult to explain only by interaction with fluids released from the peraluminous magma itself. However their source cannot be precisely determined on the base of the present data. The NYF (Nb-Y-F) signature may indicate an open system with some mantle contribution (Martin and De Vito 2005) but this hypothesis is pure speculation.

References

Budzyń, B., Harlov, D.E., Williams, M.L., Jercinovic, M.J., 2011: Experimental determination of stability relations between monazite, fluorapatite, allanite, and REE-epidote as a function of pressure, temperature, and fluid composition. *American Mineralogist, 96*, 1547-1567.

Dahlquist, J.A., 2001: REE fractionation by accessory minerals in epidote-bearing metaluminous granitoids from the Sierras Pampeanas, Argentina. *Mineralogical Magazine 65*, 463-475.

Evans, O.C., Hanson, G.N., 1993: Accessory-mineral fractionation of rare-earth element (REE) abundances in granitoid rocks. *Chemical Geology 110*, 69-93.

Hammer, J., Eidam, J., Röber, R., Ehling, B.C., 1999: Prävariszischer und variszischer granitoider Magmatismus am NE-Rand des Böhmischen Massivs - Geochemie und Petrogenese. *Zeitschrift für Geologische Wissenschaften 27*, 401-415.

Harlov, D.E., Wirth, R., Förster, H.J., 2005: An experimental study of dissolution-reprecipitation in fluorapatite: Fluid infiltration and the formation of monazite. *Contributions to Mineralogy and Petrology 15*0(3), 268-286.

Hecht, L., Thuro, K., Plinninger, R., Cuney, M., 1999: Mineralogical and geochemical characteristics of hydrothermal alteration and episyenitization in the Königshain granites, northern Bohemian Massif, Germany. *Iternational Journal of Earth Sciences 88*, 236-252.

Hoskin, P.W.O., Kinny, P.D., Wyborn, D., Chappell, B.W., 2000: Identifying accessory mineral saturation during differentiation in granitoid magmas: an integrated approach. *Journal of Petrology 41*(9), 1365-1396.

Lisowiec, K., Budzyń, B., Słaby, E., Renno, A.D., Götze, J., 2013. Fluid-induced magmatic and post-magmatic zircon and monazite patterns in granitoid pluton and related rhyolitic bodies. *Chemie der Erde 73*, 163-179.

Lisowiec, K., Budzyń, B., Słaby, E., Schulz, B., Renno, A.D., 2014. Th-U-Total Pb timing constraints on the emplacement of the granitoid pluton of Stolpen, Germany. *Acta Geologica Polonica*, submitted.

Martin, R.F., De Vito, C., 2005: The patterns of enrichment in felsic pegmatites ultimately depend on tectonic setting. *Canadian Mineralogist 43*, 2027-2048.

Uher, P., Ondrejka, M., Konečný, P., 2009: Magmatic and post-magmatic Y-REE-Th phosphate, silicate and Nb-Ta-Y-REE oxide minerals in A-type metagranite: an example from the Tuřcok massif, the Western Carpathians, Slovakia. *Mineralogical. Magazine 73*(6), 1009-1025.

Wark, D.A., Miller, C.F., 1993: Accessory mineral behavior during differentiation of a granite suite-monazite, xenotime and zircon in the Sweetwater Wash Pluton, Southeastern California, USA. *Chemical Geology 110*(1-3), 49-67.

Niobium and tantalum in accessory minerals: a review of misconceptions

Robert F. MARTIN

Earth and Planetary Sciences, McGill University, Montreal, Canada; robert.martin@mcgill.ca

Most geoscientists are quite convinced that niobium and tantalum occur in nature exclusively as Nb^{5+} and Ta^{5+}. This is certainly the way I was taught in my courses in inorganic geochemistry and crystal chemistry. Yet a chemist will tell you otherwise. Vanadium, niobium and tantalum are Group-5 elements, and share many attributes. What do we know about the valence states of vanadium in nature?

Native vanadium is found in fumaroles, Coulsonite, $Fe^{2+}V^{3+}{}_2O_4$, is a spinel-group mineral; this component accounts for the build-up in V in magnetite in the upper part of layered complexes. Tetravalent vanadium is found in duttonite, $VO(OH)_2$, which coexists with coalified tree remains in clastic sediments. The sulfide patrónite, $V^{4+}(S^{2-}{}_2)_2$, was found in organic-matter-rich shale. In more oxygenated environments, vanadium is pentavalent and adopts a tetrahedral coordination, for example in vanadinite, an apatite-group mineral. In addition, some minerals contain essential V^{3+} and V^{4+}, whereas others contain coexisting V^{4+} and V^{5+}. The valence states of vanadium seem to faithfully record the $f(O_2)$ at the time of crystallization. One sees that vanadium can be siderophile, chalcophile or lithophile, depending on environmental factors.

I attribute the impression, presumably not warranted, that Nb and Ta are exclusively found as pentavalent ions in Nature to Victor Moritz Goldschmidt, father of modern geochemistry. In his widely acclaimed treatise entitled *Geochemistry* (1954), Goldschmidt wrote pages about the "geochemical twins" Nb^{5+} and Ta^{5+}, which have the same ionic radius in spite of Ta being close to double the atomic weight of Nb. He mentioned the possibility of Nb^{4+} in passing, in half a sentence. Generations of students have learned about Nb and Ta in this way.

At last count (July 2014), there are 92 minerals in which Nb is the dominant occupant of the Nb-bearing site, and 45 minerals in which Ta is the dominant occupant of the Ta-bearing site. Whereas it is clear that oxysalt minerals with pentavalent Nb and Ta very much predominate, I shall review cases where Nb and Ta exhibit siderophile and chalcophile tendencies, just like vanadium. In fact, all three elements show evidence of promiscuous behavior.

Another misconception about these elements is that they are inert in a cooling body of granitic pegmatite. I shall review evidence that of the two elements, Ta is preferentially mobilized hydrothermally in an acidic fluid that enters the pegmatite from the exocontact. I shall also discuss the inferences made about the distribution of valence states of Nb and Ta in the mantle and core, and question how the valence state of an element can be suppressed.

It is an oversimplification, in my opinion, to believe that the accessory minerals columbite and tantalite necessarily contain only pentavalent Nb and Ta. These minerals are commonly found in a structurally disordered state in granitic pegmatites, and order can only be induced by heating to 1000°C or so. The entropy of a phase is reduced by strong heating? I shall propose a solution to this enigmatic situation that calls upon mixed valences of Nb, Ta, Fe and Mn at the time the crystals grew in the melt.

The metallogenic evolution of the Kłodzko-Złoty Stok Intrusion (Sudetes, SW Poland) in the light of a SHRIMP reconnaissance study of $\delta^{18}O$ zircon isotope composition

Stanisław Z. MIKULSKI,[1] Ewa KRZEMIŃSKA[1] and Zbigniew CZUPYT[1]

[1]*Polish Geological Institute-National Research Institute, Mineral Resources Program, Rakowiecka 4, 00-975 Warszawa; e-mail: stanislaw.mikulski@pgi.gov.pl*

The Kłodzko-Złoty Stok Granite Pluton (KZS) is located in the Sudetes, which constitute the NE margin of the Bohemian Massif. KZS consists mainly of metaluminous and minor weakly peraluminous, highly potassic I-type granitoids containing abundant mafic enclaves (e.g. Wierzchołowski 1976). Its emplacement took place in the Early Carboniferous (Viséan) during an early-plate collisional setting of thickened Variscan crust.

A U–Th–Pb investigation of KZS samples was made on the SHRIMP II at the RSES, ANU in Canberra (Mikulski *et al*. 2013). The zircon population from the KZS magmatic rocks represents various degrees of mixing/mingling between felsic and mafic magmas from hypabyssal magmatic events, involving the different compositions of granitoids and lamprophyre (spessartite) crystallizing from ca. 343 to 329 Ma. The variable modes of magma fractionation, the degree of compositional evolution and further tectonic processes may have produced different types of ore mineralization that reflected the transition from magmatic to hydrothermal environments. As an example in the area of the Ptasznik prospect, located in the southern part of KZS, with a metasomatic-type of scheelite-titanite mineralization, the granitoids have high trace element and REE contents and are enriched in incompatible elements, indicating advanced granitoid fractionation and REE enrichment. This W-Ti mineralization is younger (ca. 331 Ma; U-Pb zircon) when compared with the polymetallic auriferous ore mineralization of metasomatic type found in intimate contact with the Graniec-Bardo and Myszak apophyses that represent the earliest stage of the pluton emplacement with rocks originating from hybrid magmas (ca. 343 Ma; Mikulski and Williams 2014). The oxygen isotopic compositions of zircon provide valuable information on magma genesis. To address the genetic problems we conducted a reconnaissance study of zircon oxygen compositions on grains which previously were mounted in epoxy resin for U-Pb age investigations. About one hundred in situ analyses of oxygen isotopes were carried out on zircons from various igneous rocks and from six different localities of the KZS. Analyses were conducted on SHRIMP IIe/MC at PGI-NRI in Warsaw. They were made according to the procedures given by Ickert et al. (2008) on exactly the same spot locations as were previously measured for U-Pb. All oxygen values are reported in permil deviation relative to V-SMOW. The overall results show significant heterogeneity in $\delta^{18}O$ values, with general variation of individual spots in different rocks from −0.5‰ to +12.7‰ but the average of each sample varies from 2.48‰ to 7.22‰. Two basic zircon sample groups of oxygen isotope composition (homogeneous *vs.* heterogeneous) were recognized. The one, hosted in a tonalite from the Ptasznik area, has a moderately heavy oxygen isotopic composition and relatively narrow range in $\delta^{18}O$, with all values from 7.5‰ to 6‰ (average 7.48‰, n=14). It indicates that the melt from which the zircons precipitated included material partly derived from the crust. The other group of zircons that are hosted by a quartz-feldspar pegmatite from the Ptasznik area reveals a high variability of $\delta^{18}O$ (average 0.86‰, n=16), and documents the presence of anomalously low $\delta^{18}O$ (from +2.5 to −0.5‰) zircons, lower than a typical value for mantle-derived material (5.3‰ ± 0.6‰ 2σ) but characteristic of hydrothermal interactions. Besides, the oxygen isotope values are markedly different from those of the granite in the KZS. Such large isotopic heterogeneity

in the area is attributed to local differences in the intensity of processes caused by differences in water/rock ratio, temperature, and the proportion of meteoric vs. magmatic water, that gave rise to low-oxygen isotope fluids.

References

Ickert, R.B., Hiess, J., Williams, I. S., Holden, P., Ireland, T., R, Lanc, P., Schram, N., Foster, J., Clement, S.,W., 2008: Determining high precision, in situ, oxygen isotope ratios with a SHRIMP II: Analyses of MPI-DING silicate-glass reference materials and zircon from contrasting granite. *Chemical Geology*, *257*, 114-128.

Mikulski, S.Z., Williams, I.S., 2014: Zircon U-Pb ages of granitoid apophyses from the western part of the Kłodzko-Złoty Stok Granite Pluton (SW Poland). *Geological Quarterly, 58(2)*, 251-262.

Mikulski, S. Z., Williams, I. S., Bagiński, B., 2013: Early Carboniferous (Viséan) emplacement of the collisional Kłodzko-Złoty Stok granitoids (Sudetes, SW Poland): constraints from geochemical data and zircon U-Pb ages. *International Journal of Earth Sciences, 102,* 1007-1027.

Wierzchołowski, B., 1976: Granitoidy kłodzko-złotostockie i ich kontaktowe oddziaływanie na skały osłony (Studium petrograficzne). *Geologia Sudetica, 11*(2), 3-43.

Radiation damage in zircon: effects on chemical alteration behavior, and BSE and luminescence properties

Lutz NASDALA

Institut für Mineralogie und Kristallographie, Universität Wien, Althanstr. 14, A–1090 Vienna, Austria; e-mail: lutz.nasdala@univie.ac.at

The accumulation of self-irradiation damage in the accessory mineral zircon, $ZrSiO_4$, results in dramatic changes of this mineral's chemical and physical properties. Apart from the loss of long-range order and unit-cell swelling detected in X-ray diffraction patterns (Murakami *et al.* 1991), radiation-damaged zircon is characterized by lowered optical refraction and birefringence (Chakoumakos *et al.* 1987) and changes in elastic properties (Oliver *et al.* 1994). Increasing radiation damage is often recognized from the general depletion of luminescence emissions; for instance strongly damaged zones or interior regions typically appear dark in cathodluminescence (CL) images (Nasdala *et al.* 2002). At early damage-accumulation stages, in contrast, the luminescence of zircon may increase appreciably due to the creation of a damage-related defect center (Nasdala *et al.* 2011). The BSE (back-scattered electrons) intensity increases strongly with increasing damage (Fig. 1a), which was assigned to decreased electron-channeling in the damaged structure (Nasdala *et al.* 2006). In fact, as the BSE of natural zircon is insignificantly affected by the average atomic number (which was shown in an annealing study of cut-in-half zircon crystals by *Nasdala et al.* 2006), BSE images are virtual damage distribution maps.

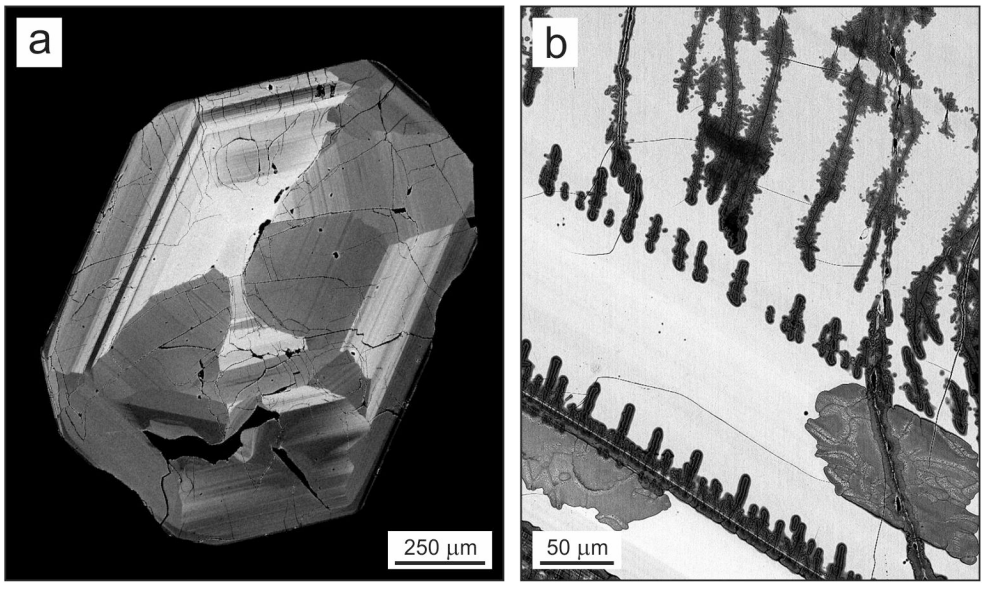

Fig. 1. Back-scattered electron images of two zircon samples. (a) Strong sector and growth zoning in a crystal from Plešovice, Czech Republic (cf. Sláma *et al.* 2008). The bright sector is particularly rich in uranium and, correspondingly, strongly radiation damaged. (b) Finger-like alteration patches in a large zircon grain from the Saranac Prospect, Bancroft, Ontario (cf. Nasdala *et al*. 2010). Fluid-driven alteration emanated from fractures and has affected preferentially more radiation-damaged growth zones. Altered areas are particularly low in BSE contrast, which is caused by their porosity.

In addition to changes in physical parameters, structural radiation damage results in generally enhanced chemical reactivity, which makes more radiation-damaged zircon grains, or interior regions within grains, more susceptible to alteration. Elevated stages of radiation damage are therefore often associated with biased U–Th–Pb ages due to the secondary loss of radiogenic Pb. Lead loss, however, occurs only if caused by an appropriate geological event, whereas even highly metamict zircon may yield concordant U–Th–Pb isotopic ratios if the specimen has spent its entire post-growth history under cool and dry conditions (Nasdala *et al.* 2002). First, chemical alteration of zircon is typically associated with the incorporation of non-formula elements that are mostly excluded in primary zircon growth, such as Ca, Fe, P, and sometimes even non-radiogenic Pb (Corfu 1987, Mathieu *et al.* 2001). Second, altered zircon is characterized by the partial loss of chemical constituents, resulting in the formation of a sub-micrometer porous texture, which in turn is recognized from very low BSE (back-scattered electrons) intensities (Fig. 1b) and deficient analytical totals (Nasdala *et al.* 2009).

The radiation damage present in a given zircon crystal, or interior region within a crystal, is the combined result of two competing processes, namely (i) accumulation of structural defects that are created in cascades of atomic knock-ons, and (ii) structural reconstitution due to thermal annealing. Damage accumulation is hence strongly temperature-dependent, controlled by the ratio of the two processes above (Nasdala *et al.* 2001). Quantitative estimates of the degree of damage retention in unknown zircon is possible by comparing the present damage with the theoretical maximum damage; the latter being determined from zircon samples that have not experienced thermal annealing. Two examples are shown in Fig. 2. The plot of the Raman-band broadening (quantifying the present damage) against time-integrated alpha doses shows that data pairs for the Plešovice zircon plot close to the trend defined by zircon samples that are believed to represent nearly complete accumulation of the alpha-event damage (Nasdala *et al.* 2001). This suggests that the Plešovice zircon has stored the majority of radiation damage since crystal growth (Sláma *et al.* 2008). Sri Lankan gem zircon, in contrast, is only about half as radiation-damaged as would correspond to complete damage accumulation, indicating a significant annealing history (Nasdala *et al.* 2004). More examples, including those of a recent study of zircon xenocrysts from kimberlites (Nasdala *et al.* 2014), are presented and discussed in detail.

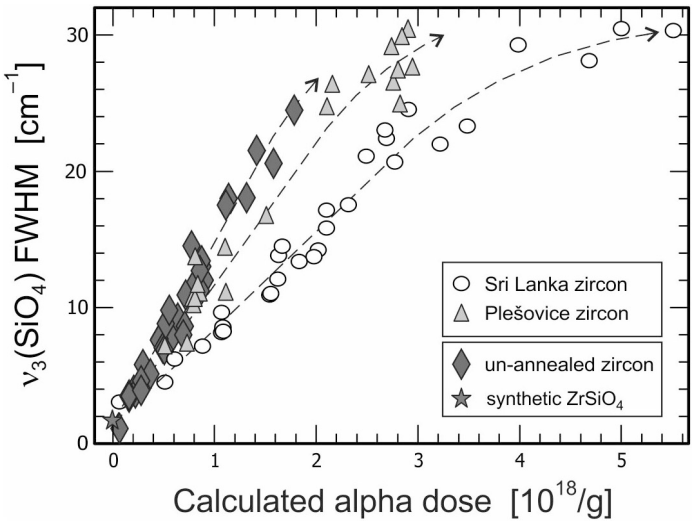

Fig. 2. Broadening (FWHM = full width at half-maximum) of the $\nu_3(SiO_4)$ Raman band (B_{1g} mode at ~1000 cm^{-1}) plotted against self-irradiation dose. Data sources: Murakami *et al.* (1991; doses), Zhang *et al.* (2000; Raman), and Nasdala *et al.* (2004) for Sri Lanka; Sláma *et al.* (2008) for Plešovice; Nasdala *et al.* (2001) for unannealed zircon; Nasdala *et al.* (2002) for synthetic $ZrSiO_4$.

References

Chakoumakos, B.C., Murakami, T., Lumpkin, G.R., Ewing, R.C., 1987: Alpha-decay-induced fracturing in zircon: the transition from the crystalline to the metamict state. *Science, 236*, 1556-1559.

Corfu, F., 1987: Inverse age stratification in the archaean crust of the superior province: Evidence for infra- and subcrustal accretion from high resolution U-Pb zircon and monazite ages. *Precambrian Reearch*, *36*, 259-275.

Mathieu, R., Zetterström, L., Cuney, M., Gauthier-Lafaye, F., Hidaka, H., 2001: Alteration of monazite and zircon and lead migration as geochemical tracers of fluid paleocirculations around the Oklo-Okélobondo and Bangombé natural nuclear reaction zones (Franceville basin, Gabon). *Chemical Geolology*, *171*, 147-171.

Murakami, T., Chakoumakos, B.C., Ewing, R.C., Lumpkin, G.R., Weber, W.J., 1991: Alpha-decay event damage in zircon. *American Mineralogist, 76*, 1510-1532.

Nasdala, L., Wenzel, M., Vavra, G., Irmer, G., Wenzel, T., Kober, B., 2001: Metamictisation of natural zircon: accumulation versus thermal annealing of radioactivity-induced damage. *Contribution to Mineralogy and Petrology, 141*, 125-144.

Nasdala, L., Lengauer, C.L., Hanchar, J.M., Kronz, A., Wirth, R., Blanc, P., Kennedy, A.K., Seydoux-Guillaume, A.-M., 2002: Annealing radiation damage and the recovery of cathodoluminescence. *Chemical Geolology*, *191*, 121-140.

Nasdala, L., Reiners, P.W., Garver, J.I., Kennedy, A.K., Stern, R.A., Balan, E., Wirth, R., 2004: Incomplete retention of radiation damage in zircon from Sri Lanka. *American Mineralogist, 89*, 219-231.

Nasdala, L., Kronz, A., Hanchar, J.M., Tichomirowa, M., Davis, D.D., Hofmeister, W., 2006: Effects of natural radiation damage on back-scattered electron images of single-crystals of minerals. *American Mineralogist, 91*, 1739-1746.

Nasdala, L., Kronz, A., Wirth, R., Váczi, T., Pérez-Soba, C., Willner, A., Kennedy, A.K., 2009: Alteration of radiation-damaged zircon and the related phenomenon of deficient electron microprobe totals. *Geochimica at Cosmochimica Acta, 73*, 1637-1650.

Nasdala, L., Hanchar, J.M., Rhede, D., Kennedy, A.K., Váczi, T., 2010: Retention of uranium in complexly altered zircon: An example from Bancroft, Ontario. *Chemical. Geology, 269*, 290-300.

Nasdala, L., Grambole, D., Götze, J., Kempe, U., Váczi, T., 2011: Helium irradiation study on zircon. *Contribution to Mineralogy and Petrology, 161*, 777-789.

Nasdala, L. Kostrovitsky, S., Kennedy, A.K., Zeug, M., Esenkulova, S.A., 2014: Retention of radiation damage in zircon xenocrysts from kimberlites, Northern Yakutia. *Lithos, 206-207*, 252-261.

Oliver, W.C., McCallum, J.C., Chakoumakos, B.C., Boatner, L.A., 1994: Hardness and elastic modulus of zircon as a function of heavy-particle irradiation dose: II. Pb-ion implantation damage. *Radiation Effects and Defects in Solids, 132*, 131-141.

Sláma, J., Košler, J., Condon, D.J., Crowley, J.L., Gerdes, A., Hanchar, J.M., Horstwood, M.S.A., Morris, G.A., Nasdala, L., Norberg, N., Schaltegger, U., Tubrett, M.N., Whitehouse, M.J., 2008: Plešovice zircon—a new natural reference material for U-Pb and Hf isotopic microanalysis. *Chemical Geolology, 249*, 1-35.

Zhang, M., Salje, E.K.H., Farnan, I., Graeme-Barber, A., Daniel, P., Ewing, R.C., Clark, A.M., Lennox, H., 2000: Metamictization of zircon: Raman spectroscopic study. *Journal of Physics: Condensed Matter, 12*, 1915-1925.

A new nomenclature proposal for the samarskite-group minerals: a draft on the basis of geochemical relationships

Adam PIECZKA

Department of Mineralogy, Petrography & Geochemistry, AGH – University of Science & Technology, Mickiewicza 30, 30-059 Cracow; pieczka@agh.edu.pl

The samarskite group (SG) comprises a group of commonly completely metamict and pervasively altered U–Y–*REE*–Fe–Ca niobates of general stoichiometry ABO_4 (Sugitani *et al.* 1985, Warner and Ewing 1993), where *A* and *B* sites have octahedral coordination and are distinctive in the different sizes of the occupants. The *A* site is occupied by larger cations U^{4+}, Th^{4+}, Y^{3+}, REE^{3+}, Fe^{2+}, Fe^{3+} and Ca^{2+} with minor Na^{+}, Mg^{2+}, Al^{3+}, K^{+}, Mn^{2+}, Zr^{4+}, Sn^{4+}, W^{6+} and Pb^{2+}, whereas the *B* site is occupied dominantly by Nb^{5+}, minor Ta^{5+} and Ti^{4+} (Nielsen 1970, Sugitani *et al.* 1985, Warner and Ewing 1993). Iron can be present as Fe^{2+} and Fe^{3+}, accepted as the *A*-site occupants, except where a deficiency of Nb+Ta+Ti is completed by Fe^{3+}. Fe^{2+} or Fe^{3+} can even dominate the *A*-site population; however, the respective end-members are not distinguished mainly because the Fe^{2+} and Fe^{3+} contents calculated by charge-balance may represent *post*-metamictization values (Hanson *et al.* 1998). Ti^{4+} commonly is related to the *B* site, but in the case of a high sum of the *B*-site cations, it can be also located at the *A* site (Sugitani *et al.*1985, Warner and Ewing 1993). As Nb^{5+} is almost always the dominant *B*-site cation, mineral species in the SG are defined by the dominant *A*-site cation (Hanson *et al.* 1999): $\underline{U^{4+}}$ in **ishikawaite**, $(U,Fe,Y,Ca)(Nb,Ta)O_4$ (Kimura 1922, Fleischer and Mandarino 1995), $\underline{Y^{3+}+REE^{3+}}$ in **samarskite-(Y)**, $(Y,REE,U,Fe^{3+})(Nb,Ta)O_4$ (Sugitani *et al.* 1985, Hanson *et al.* 1988, 1989), $\underline{Yb^{3+}+Y^{3+}+ REE^{3+}}$ in **samarskite-(Yb)**, $(Yb,Y, REE,U,Ca, Fe^{2+})NbO_4$ (Simmons *et al.* 2006), and $\underline{Ca^{2+}}$ in **calciosamarskite**, $(Ca,Fe,Y)(Nb,Ta,Ti)O_4$ (Ellsworth 1928, Fleischer and Mandarino 1995). The existing simple classification of the samarskite-group minerals is very imperfect. Hanson *et al.* (1999), who, proposed this nomenclature, were aware of its imperfections, and in their paper they wrote that '… defining samarskite-group minerals is more complex than this simple ternary [*i.e.*, Y+*REE* – U+Th – Ca)] relation suggests because iron (Fe^{2+} and/or Fe^{3+}) is often an abundant *A*-site cation', and further '… the presence of iron (Fe^{2+} or Fe^{3+}) as a dominant *A*-site cation cannot be ignored'.

The results presented of crystal-chemical relationships between the *A*- and *B*-site cations have been studied on a set of 506 EMP analyses, representing minerals of the SG in terms of the canonical CV1 and CV2 values of the *three-group model* of Ercit (2005). The set comprised 200 analyses of SGM from the Piława pegmatitic system in the Góry Sowie block, Poland (Pieczka *et al.* 2014); 295 analyses from Warner and Ewing (1993); 5 analyses from Hanson *et al.* (1998); 4 analyses from Hanson *et al.* (1999); and the analysis of the type samarskite-(Yb) (Simmons *et al.* 2006) and samarskite-(Y) by Tomašić *et al.* (2012). All compositions were normalized in relation to 4 O or 4(O,OH) *pfu*, with the assumption of valence charge-balance and a value of Fe^{3+}/Fe_{total} ratio such as to reduce excesses in the cation totals over two structurally available sites.

Already the simple presentation of the data in the ${}^{A}R^{2+}–{}^{A}R^{3+}–{}^{A}R^{4+}$ triangle (Fig. 1) points to minerals of the samarskite group being a solid solution between two groups of end-members: $R^{3+}NbO_4$ and $(R^{4+}_{0.5}R^{2+}_{0.5})NbO_4$. A detail analysis of possible substitutions and the average *A*-site population radius has allowed an evaluation of the following possible end-members in the SG:

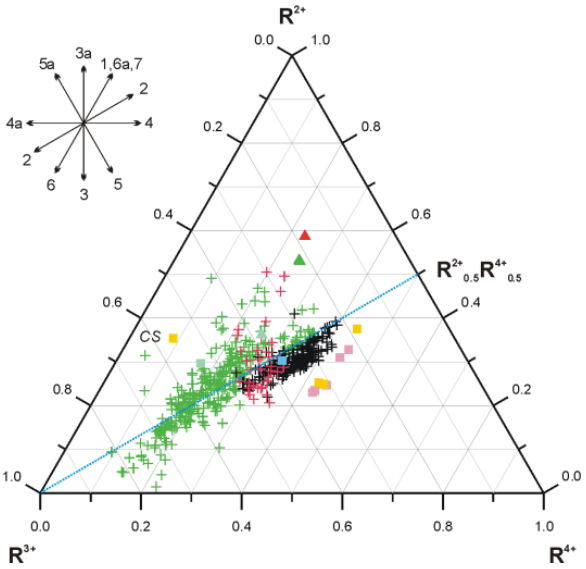

Fig. 1. Compositional plot of the studied SG and pyrochlore-group compositions in the ternary diagram ${}^{A}R^{2+}$–${}^{A}R^{3+}$–${}^{A}R^{4+}$. Symbols: dark crosses – OH-free analyses of SGM from Piława Górna, red crosses – OH-containing analyses of SGM from Piława Górna, green crosses – analyses by Warner and Ewing (1993), pink squares – analyses by Hanson *et al.* (1998), yellow squares – analyses by Hanson *et al.* (1999), blue square – samarskite-(Yb) by Simmons *et al.* (2006), light greenish square – samarskite-(Y) and *altered samarskite* by Tomašić *et al.* (2012), green triangles – PGM (243/4 and 5) by Warner and Ewing (1993), red triangle – a PGM accompanying a sample of samarskite-(Y) from Piława Górna. Dotted line – a compositional trend in the $R^{3+}NbO_4$–$(R^{4+}_{0.5}R^{2+}_{0.5})NbO_4$ solid solution.

$(Y^{*}_{0.5}Fe^{3+}{}^{*}_{0.5})NbO_4$, $[(U^{*}_{0.25}Ca_{0.25})Fe^{3+}{}^{*}_{0.5}]NbO_4$, $[(Y^{*}_{0.5}Fe^{2+}{}^{*}_{0.25}Ti^{*}_{0.25})]NbO_4$, $(U^{*}_{0.5}Fe^{2+}{}^{*}_{0.5})NbO_4$, $(Y^{*}_{0.5}Fe^{2+}{}^{*}_{0.5})(Nb_{0.5}W_{0.5})O_4$, $(Fe^{2+}{}^{*}_{0.5}U^{*}_{0.25}Ca_{0.25})(Nb_{0.5}W_{0.5})O_4$, $(U^{*}_{0.5}Fe^{2+}{}^{*}_{0.5})(Ti_{0.5}W_{0.5})O_4$ for Nb+Ta+W = 1 *apfu*, + $(U^{*}_{0.5}Fe^{3+}{}^{*}_{0.5})(Nb_{0.5}Ti_{0.5})O_4$, $(Y^{*}_{0.5}Ti^{*}_{0.5})(Nb_{0.5}Ti_{0.5})O_4$, $(U^{*}_{0.5}Ti^{*}_{0.5})TiO_4$ and $(U^{*}_{0.5}Fe^{3+}{}^{*}_{0.5})(Nb_{0.75}Fe^{3+}{}_{0.25})O_4$ for Nb+Ta+W < 1 *apfu* when Ti completes the deficiency, + $(Y^{*}_{0.5}Fe^{2+}{}^{*}_{0.33}Nb_{0.17})NbO_4$ for Nb+Ta+W > 1 apfu, when an excess of Nb occurs at the *A* site. In this light, minerals of the samarskite group can be treated as solid solutions between the fergusonite-group (FG) end-members and ixiolite-, wolframite-, rutile- and ferrocolumbite species with the ratio 1 : 1. An ideal theoretical formula of the group may be presented as $A1_{0.5}A2_{0.5}[(Nb,Ta,W,Ti)O_4]$, where *A1* and *A2* represent the same structural position filled with cations of two different populations: *A1* = Ca^{2+}, Y^{3+}* [=Sc^{3+},Y^{3+},*REE*$^{3+}$,(U^{4+}*+Ca^{2+})/2], U^{4+}* (=U^{4+},Th^{4+}), and *A2* = Fe^{2+}* (= Fe^{2+},Mn^{2+},Mg^{2+}), Fe^{3+}* [=Fe^{3+},Al^{3+},(Fe^{2+}*+Ti^{4+}*)/2], Ti^{4+}* (Ti^{4+},Zr^{4+},Sn^{4+}) ± Nb^{5+}. Complete disordering of both group cations at the *A* site supports [6]-fold coordination around the site. An excess of Ca can be a sign of late crystallization under the action of, or metasomatic alteration induced by, Ca-bearing fluids, forming first $[(U_{0.25}Ca_{0.25})Fe^{3+}]NbO_4$ species of SG, further $(U_{0.5}Ca_{0.5})NbO_4$ species of FG, and finally $CaNbO_3(OH)$ = 1/2 $Ca_2Nb_2O_7 \cdot H_2O$ species of the pyrochlore group.

A new classification of the samarskite group is necessary because the one currently used is very imperfect due to the omission of ${}^{A}Fe^{2+}$ and ${}^{A}Fe^{3+}$, commonly abundant and sometimes even dominant cations in the *A*-site population of the SG species. This results in a very imperfect classification, very often on the basis only of 40–60% of the *A*-site population. The classification also does not take into consideration the presence of Ti and W at the *B* site or Nb at the *A* site. The proposed classification includes all the compositional details.

References

Ellsworth, H.V., 1928: A mineral related to samarskite from the Woodcox Mine, Hybla Ontario. *American Mineralogist, 13*, 63–65.

Ercit, T.S., 2005: Identification and alteration trends of granitic-pegmatite-hosted (Y,REE,U,Th)–(Nb,Ta,Ti) oxide minerals: a statistical approach. Canadian Mineralogist, 43, 1291–1303.

Fleischer, M., Mandarino, J.A., 1995: Glossary of Mineral Species 1995. The Mineralogical Record, Tuscon, Arizona, 280 pp.

Hanson, S.L., Simmons, W.B. Jr., Falster, A.U. 1998: Nb–Ta–Ti oxides in granitic pegmatites from the Topsham pegmatite district, Southern Maine. *Canadian Mineralogist, 36*, 601-608.

Hanson, S.L., Simmons, W.B., Falster, A.U., Foord, E.E., Lichte, F.E., 1999: Proposed nomenclature for samarskite-group minerals: new data on ishikawaite and calciosamarskite. *Mineralogical Magazine, 63*, 27-36.

Kimura, K., 1922: Ishikawaite: a new mineral from Ishikawa, Iwaki. *Journal of the Geological Society, Tokyo, 29*, 316-320 (in Japanese).

Nilssen, B., 1970: Samarskites: Chemical composition, formula and crystalline phases produced by heating. Norsk *Geologisk Tidsskrift, 50*, 357-373.

Pieczka, A., Szuszkiewicz, A., Szełęg, E., Ilnicki, S., Nejbert, K., Turniak, K., 2014: Samarskite-group minerals and alteration products: an example from the Julianna pegmatitic system, Piława Górna, SW Poland. *Canadian Mineralogist, 52*, 303-319.

Simmons, W.B., Hanson, S.R., Falster, A.U., 2006: Samarskite-(Yb): A New species of the samarskite group from the Little Patsy pegmatite, Jefferson County, Colorado. *Canadian Mineralogist, 44*, 1119-1125.

Sugitani, Y., Suzuki, Y., Nagashima, K., 1985: Polymorphism of samarskite and its relationship to other structurally related Nb-Ta oxides with the αPbO_2 structure. *American Mineralogist, 70*, 856-866.

Tomašić N., Gajović, A., Bermanec, V., Linarić, M.R., SU, D., Škoda, R., 2012: Preservation of the samarskite structure in a metamict ABO4 mineral: a key to crystal structure identification. *European Journal of Mineralogy, 22*, 435-442.

Warner, J.K., Ewing, R.C., 1993: Crystal chemistry of samarskite. *American Mineralogist, 78*, 419-424.

Fluid-mediated re-equilibration and self-irradiation in complex U-Th-rich assemblages of pegmatites: a case from Norway and implications for U-Th-Pb dating of ore deposits

Anne-Magali SEYDOUX-GUILLAUME [1], Bernard BINGEN[2], Carley DURAN[3], Valérie BOSSE[4], Jean-Louis PAQUETTE[4], Damen GUILLAUME[1], and Philippe de PARSEVAL[1], and Jannick INGRIN[5]

[1]GET, UMR5563 CNRS-UPS-IRD, Université de Toulouse, 14 av E. Belin, 31400 Toulouse, France ; anne-magali.seydoux@get.obs-mip.fr
[2]Geological Survey of Norway, 7491 Trondheim, Norway
[3] Département des sciences appliquées, 555 Boulevard de l'Université, Chicoutimi, Québec, Canada, G7H 2B1
[4]LMV, Université Blaise Pascal, 5 rue Kessler, 63000 Clermont-Ferrand, France
[5]UMET, UMR 8207 CNRS, Université Lille1, 59655 Villeneuve d'Ascq, France

In most rocks, uranium and thorium are concentrated in favorable crystallographic sites in a few minerals such as zircon, monazite, titanite, and rarely uraninite, thorianite, thorite/huttonite, euxenite. These minerals are submitted to intense self-irradiation that can lead to amorphization and also modify their environment by irradiating the host minerals. Here, we focus on accessory minerals in rare-metal-rich pegmatites from southern Norway (Kragerø, Iveland-Evje); some of these minerals are rich in U (e.g. up to 15wt% for euxenite). A complex paragenesis of zircon + monazite + xenotime + euxenite was studied by multiple methods including optical and electron microscopy and U-Pb geochronology (SIMS and LA-ICP-MS). Observations show that complex relationships exist between the different minerals (especially zircon-euxenite) and the various processes (alteration by fluids and radiation effects) which have repercussions on the U-Th-Pb geochronology response. Irradiation (self and out), destroys the crystal lattice (amorphization), promoting alteration of the more or less destroyed parts. Amorphization induces volume increase, leading to the formation of cracks which eventually connected into a network through the rock. This fracturing allows fluid circulation, and promotes alteration of source minerals and dispersion of elements (e.g. Pb and U). Our results demonstrate, however, that monazite and xenotime crystals, even altered, have a greater potential for U-Th-Pb dating (Seydoux-Guillaume *et al.* 2012).

References

Seydoux-Guillaume, A.-M., Montel, J.-M., Bingen, B., Bosse, V., de Parseval, P., Paquette, J.-L., Janots, E., Wirth, R., 2012: Low-temperature alteration of monazite: Fluid mediated coupled dissolution-precipitation, irradiation damage, and disturbance of the U-Pb and Th-Pb chronometers. *Chemical Geology, 330-331*, 140-158.

Merrillite and apatite from NWA 2975 shergottite: TEM and chemical-composition study

Ewa SŁABY[1], Monika KOCH-MÜLLER[2], Richard WIRTH[2], Hans-Jürgen FÖRSTER[2], Anja SCHREIBER[2], Ulrich SCHADE[3], Dieter RHEDE[2]

[1]*Institute of Geological Sciences, Polish Academy of Sciences, Research Centre in Warsaw, Twarda 51/55, 00-818 Warsaw, Poland, e-mail: e.slaby@twarda.pan.pl,*
[2]*Deutsches GeoForschungs Zentrum, Telegrafenberg, 14473 Potsdam, Germany,*
[3]*Helmholtz-Zentrum Berlin, Elektronenspeicherring BESSY II, Albert-Einstein-Str. 15, 12489 Berlin, Germany*

Phosphates, such as volatile-bearing apatite and anhydrous merrillite, are frequently used to decipher magma composition. In NWA 2975, merrillite represents intermediate merrillite-–ferromerrillite solid solutions and fluorapatite is rich in Cl and water. We combined the focused ion beam sample preparation technique with polarized synchrotron-based FTIR- and Laser-Raman-spectroscopy to determine structurally bound OH, F, Cl and CO_3-groups in apatite from NWA 2975 shergottite. These are the first FTIR spectra in the OH-stretching region from a Martian apatite showing the characteristic OH-bands of a F-rich, Cl- and H_2O-bearing apatite. The FTIR-based quantification of the incorporated H_2O is in good agreement with the H_2O concentration estimated by combining electron-microprobe analyses of F and Cl with mineral stoichiometry. The process of the crystallization of apatite coexisting with merrillite is reconstructed from TEM and geochemical analyses. Both phosphates have been indexed (HR TEM study). They reveal planar deformations or mosaics of several, variably distorted and undistorted sub-domains reflecting shock-induced deformation, suggesting that both species precipitated from residual magma prior to the shock event. Quenched, very porous melt drops of phosphate composition, containing silica and volatiles (with F predominating over Cl) occur in merrillite, but not in apatite. In apatite cracks, crystallization of residual, F-enriched and Cl-free melt is observed. Tiny, tile-shaped crystals (indexed as apatite) nucleated on the crack walls and grew in parallel-oriented piles. The composition of host apatite shows the presence of both F and Cl in the parental magma. Two apatite generations support the occurrence of volatiles in the melt during phosphate formation. Geochemical modelling shows that the parental magma was volatile-poor. Volatile concentrations increased considerably during progressive fractional crystallization; however, Cl was mostly exhausted before its termination. The analyses show that the volatile budget recognized in apatite can be related with a high probability to a magmatic origin, and was not altered during post-magmatic events. The relative proportions of halogen and water in apatite indicates a high-temperature parental magma with high F activity and comparatively low Cl and water activity ($F>>Cl\sim H_2O$). The model supposed for Amazonian magmatism (the age of NWA 2975 is 304 ± 29 Ma; Lindsay *et al.* 2013) by Balta and McSween (2013) assumes a dry upper mantle with occasional entrainment of hydrous material from a wet lower mantle. Thus volatile-enriched reservoirs may contribute to shergottite magma generation. The volatile budget estimated for NWA 2975 apatite rather points to a volatile-poor mantle as a shergottite magma source.

References

Lindsay F.N., Osmond J., Delaney J.S., Herzog G.F., Turrin B., Park J., and Swisher C.C. III, 2013: Ar/Ar Systematics of Martian Meteorite NWA 2975. 44th Lunar and Planetary Science Conference, 2911.

Balta J.B., and McSween Jr., H.Y., 2013: Water and the composition of martian magmas. *Geology, 41*, 1115-111.

Structural relationships in chevkinite and perrierite

Marcin STACHOWICZ[1,2], Krzysztof WOŹNIAK[2], Bogusław BAGIŃSKI[3], Ray MACDONALD[3]

[1]*College of Inter-Faculty Individual Studies in Mathematics and Natural Sciences (MISMaP), Żwirki i Wigury 93, 02-089 Warsaw, Poland; email: marcin.stachowicz@chem.uw.edu.pl*
[2]*Biological and Chemical Research Centre, Chemistry Department, University of Warsaw, Żwirki i Wigury 101, 02-089 Warsaw, Poland*
[3]*Institute of Mineralogy, Geochemistry and Petrology, University of Warsaw, 02-089, al. Żwirki i Wigury 93, Warsaw, Poland*

The chevkinite group of minerals (dominated by chevkinite and perrierite) is increasingly being recognized as accessory phases in a wide range of igneous and metamorphic rocks. The general formula for the most common members of the group, is $A_4BC_2D_2(Si_2O_7)_2O_8$, where the most common cations in each site are A = Ca^{2+}, REE^{3+} (Rare Earth Elements), Sr^{2+}, Th^{4+}; B = Fe^{2+}; C = Fe^{2+}, Fe^{3+},Ti^{4+}, Al^{3+}, Mn^{2+}, Mg^{2+}; and D = Ti^{4+}. A detailed study of crystal structures obtained from single crystal X-ray diffraction experiments will be presented.

A rational allocation of ions to particular sites in the perrierite and chevkinite crystal structures is proposed. Our approach is based on the use of mean ionic radii, together with electron charge density and polyhedral volumes. Additionally, the final structure is checked using a Charge Density model (CD), a method complementary to the commonly used Bond Valence approach (BV). The advantages of this method are that it allows for calculations of coordination number or bond weights even in the case of occupational disorder or the presence of a distortion of the first coordination spheres.

As well as the difference in the β angle of the unit cell between perrierite and chevkinite, there is a difference in the packing of some ions. The distortion of the central ion in one of the octahedra (DO_6 in the general formula), which is present in all perrierites, is rationalised in terms of interatomic interactions between closely located cations. The influence of temperature and pressure on the crystal structures of different minerals from the group was analyzed. A phase transition brought by annealing for 24h at 750°C in an argon atmosphere was observed. High pressure experiments were carried out on single crystal X-ray diffractometer equipped with a Merill-Bessett diamond anvil cell. Finally an experimental verification of Fe and Ti oxidation states by photoelectron spectroscopy was introduced. The results are compared with theoretical calculations (BV, CD).

Th, U, S and As enrichment in monazite-group minerals: a product of primary magmatic/metamorphic vs. secondary alteration processes.

Pavel UHER[1]

[1]*Department of Mineralogy and Petrology, Comenius University, Mlynská dolina G, 842 15 Bratislava, Slovakia; e-mail: puher@fns.uniba.sk*

Introduction

Monazite is one of the most widespread accessory minerals and the most important carriers of rare-earth elements (REE; La to Lu and Y) in Si-rich magmatic and metamorphic rocks (especially granitic rocks *s.l.* and their volcanic equivalents, pegmatites, orthogneisses, metapelites to metapsammites, and some hydrothermal assemblages). The end-member formula of the most common natural monazite member, monazite-(Ce), could be written as $CePO_4$, and La-, Nd-, and Sm-dominant species have also been rarely described. Moreover, natural monazites show very wide compositional variations due to significant admixtures of actinide elements (Th and U) together with Ca, Sr and Si, as well as S and As. These variations reflect specific genetic conditions of monazite origin and they represent a very useful tool for understanding the host rock evolution.

Th and U in monazite

Natural monazite-(Ce) usually contains Th^{4+}, a cation that partly replaces REE through two basic heterovalent isomorphic mechanisms: (1) $Th^{4+} + Si^{4+} = REE^{3+} + P^{5+}$ or $ThSiREE_{-1}P_{-1}$ (huttonite-type substitution), and (2) $Ca^{2+} + Th^{4+} = 2REE^{3+}$ or $CaThREE_{-2}$ (cheralite-type substitution). Therefore, the Th content in monazite reaches up to 30 wt% ThO_2 and monazite to huttonite ($CePO_4$-$ThSiO_4$) and monazite to cheralite ($CePO_4$-$Ca_{0.5}Th_{0.5}PO_4$) solid solutions have been described in numerous natural compositions (e.g., Förster 1998, Williams *et al.* 2007). Both substitutions are allowed by the similarity of the cation radii and other geochemical properties of Th^{4+} and light REE^{3+} (LREE). The monoclinic monazite-type structure with a dominance of large LREE cations (mainly La^{3+} to Sm^{3+}) in nine-fold coordination and effective ionic radii of 1.13 to 1.22 . 10^{-10} m (Shannon 1976), prefers the larger $^{[9]}Th^{4+}$ (1.09 . 10^{-10} m), over the smaller $^{[9]}U^{4+}$ (1.05 . 10^{-10} m), which prefers the tetragonal xenotime-(Y) and zircon structure with a dominance of smaller heavy REE cations (HREE, Y^{3+} and Gd^{3+} to Lu^{3+}).

Consequently, U-rich monazite (UO_2 >1 wt%) is relatively rare in nature. It has been described from granitic pegmatites from Italian Alps, where UO_2 occasionally reaches 12 to 16 wt% (Gramaccioli and Segalstad 1978, Mannucci *et al.* 1986), and from some granitic rocks (3 to 14 wt% UO_2; e.g., Bea 1996, Förster 1998, Appel *et al.* 2011, Uher *et al.* 2013). The highest U concentrations (up to 23 wt% UO_2, 0.2 apfu U) are in monazite from the Belvís de Monroy granite, Spain (Pérez-Soba *et al.* 2014). The entry of U into the monazite structure is compensated mainly by Ca ($Ca^{2+} + U^{4+} = 2REE^{3+}$ or $CaUREE_{-2}$) substitution; the $U^{4+} + Si^{4+} = REE^{3+} + P^{5+}$ ($USiREE_{-1}P_{-1}$) mechanism is negligible. The presence of the $Ca_{0.5}U_{0.5}PO_4$ molecule in natural monazite is corroborated by the existence of its synthetic monoclinic analogue with a monazite structure (Dusausoy *et al.* 1996, Bregiroux *et al.* 2007, Terra *et al.* 2008).

S and As in monazite

Both S and As replace P in the tetrahedral $(PO_4)^{3-}$ anionic group of monazite by three possible substitution mechanisms: (1) $(Ca,Sr)^{2+} + (SO_4)^{2-} = REE^{3+} + (PO_4)^{3-}$ or $(Ca,Sr)SREE_{-1}P_{-1}$, (2) $(SiO_4)^{4-} + (SO_4)^{2-} = 2(PO_4)^{3-}$ or $SiSP_{-2}$, and (3) $(AsO_4)^{3-} = (PO_4)^{3-}$ or AsP_{-1}.

The highest S and Sr contents in natural monazite (up to 11 wt% SO_3, 0.3 apfu S and up to 9 wt% SrO, 0.2 apfu Sr) have been reported from the Bacúch metamorphic magnetite deposit, Slovakia (Pršek *et al.* 2010). In addition, S(Sr)-rich monazites (5 to 9 wt% SO_3 and up to 5 wt% SrO) have been described in altered rhyolites (Ondrejka *et al.* 2007), mylonitic mica schists and aplites (Krenn *et al.* 2008), and calcite kimberlites (Chakhmouradian and Mitchell 1999). The $(Ca,Sr)SREE_{-1}P_{-1}$ substitution is dominant for all these occurrences, whereas the $SiSP_{-2}$ mechanism plays a negligible role, if any. The existence of a monoclinic $CaSO_4$ polymorph with a monazite-type structure ("clinoanhydrite", Ondrejka *et al.* 2007) is confirmed by the phase transition of anhydrite (orthorhombic $CaSO_4$) to a monazite-structure compound under (ultra)high-pressure conditions, over 2 GPa (Crichton *et al.* 2005, Bradbury and Williams 2009). However, structural dissimilarities among $CePO_4$, and $CaSO_4$ or $SrSO_4$, arising from the differences in ionic radii of $LREE^{3+}$ relative to Ca^{2+} or Sr^{2+} (Shannon 1976), limit the incorporation of these elements to specific conditions.

Arsenic occurs in very low concentrations in common monazite, usually below 0.2 wt% As_2O_5. Nevertheless, nearly complete solid solution between monazite-(Ce) and isostructural gasparite-(Ce) $CeAsO_4$ was described in altered rhyolite near Tisovec, Slovakia (Ondrejka *et al.* 2007). These results reveal a broad miscibility range of both monazite to gasparite and associated xenotime to chernovite (YPO_4-$YAsO_4$) solid solutions, where atomic As/(As+P) ratios attain 0.00 to 0.73 and 0.10 to 0.94, respectively.

Concluding remarks: Primary magmatic/metamorphic or secondary origin of Th-, U-, S- and As-rich monazite

Th-rich monazite occurs in various genetic conditions. The content of the huttonite molecule in magmatic monazite generally increases with increase in temperature; however occurrences of pegmatitic or post-magmatic huttonite have also been reported (Broska *et al.* 2000, Harlov *et al.* 2007). Monazite to cheralite solid solution occurs mainly in late-magmatic to early post-magmatic assemblages, in more evolved granitic rocks (mainly of S- and A-type tendency) and pegmatites, where the presence of fluxing and volatile elements (F, H_2O, Li, Be, B, P) and rock-fluid interaction play an important role (e.g., Bea 1996, Förster 1998).

Highly U-rich monazite (in association with U-rich xenotime and P-rich zircon) probably originated in specific peraluminous, low-Ca and high-P evolved granitic melts due to the combination of the high solubility of apatite, where U is preferably incorporated into monazite structure by the $CaUREE_{-2}$ substitution (Pérez-Soba *et al.* 2014).

On the other hand, precipitation of S- and As-rich monazite is connected with secondary, post-magmatic or post-metamorphic and rather low-temperature (hydrothermal), fluid-driven processes. For example, sulfatian monazite forms apparent overgrowths on primary metamorphic S-poor monazite at Bacúch (Pršek *et al.* 2010) and a secondary origin has also been proposed for other occurrences of S-rich monazite (Chakhmouradian and Mitchell 1999, Krenn *et al.* 2008). As-rich monazite-(Ce) to gasparite-(Ce) originated during the post-magmatic alteration of primary monazite by As-rich fluids at high fO_2 conditions (Ondrejka *et al.* 2007).

Acknowledgements: This work was supported by the VEGA grant No. 1/0257/13.

Rererences

Appel, P., Cirrincione, R., Fiannacca, P., Pezzino, A., 2011: Age constraints on Late Paleozoic evolution of continental crust from electron microprobe dating of monazite in the Peloritani Mountains (southern Italy): Another example of resetting of monazite ages in high-grade rocks. *International Journal of Earth Sciences, 100(1)*, 107-123.

Bea, F., 1996: Residence of REE, Y, Th and U in granites and crustal protoliths; implications for the chemistry of crustal melts. *Journal of Petrology, 37*(3*)*, 521-552

Bradbury, S.E, Williams, Q., 2009: X-ray diffraction and infrared spectroscopy of monazite-structured $CaSO_4$ at high pressures: Implications for shocked anhydrite. *Journal of Physics and Chemistry of Solids, 70*, 134-141.

Bregiroux D., Terra O., Audubert F., Dacheux N., Serin V., Podor R., Bernache-Assollaut D., 2007: Solid-state synthesis of monazite-type compounds containing tetravalent elements. *Inorganic chemistry, 46*(*24*), 1372-10382.

Broska I., Petrík I., Williams C.T. 2000: Coexisting monazite and allanite in peraluminous granitoids of the Tribeč Mountains, Western Carpathians. *American Mineralogist 85*, 22-32.

Chakhmouradian A., Mitchell R.H. 1999: Niobian ilmenite, hydroxylapatite and sulfatian monazite: Alternative hosts for incompatible elements in calcite kimberlite from Internatsional'naya, Yakutia, Source of the Document. Canadian *Mineralogist, 37*(*5*), 1177-1189.

Crichton W.A., Parise J.B., Antao S.M., Grzechnik A. 2005: Evidence for monazite-, barite-, and $AgMnO_4$ (distorted barite)-type structures of $CaSO_4$ at high pressure and temperature. *American Mineralogist, 90*, 22-27

Dusausoy Y., Ghermani N.-E., Podor R., Cuney M., 1996: Low-temperature ordered phase of $CaU(PO_4)_2$: Synthesis and crystal structure. *European Journal of Mineralogy, 8*, 667-673

Förster H.-J.,1998: The chemical composition of REE-Y-Th-U-rich accessory minerals in peraluminous granites of the Erzgebirge-Fichtelgebirge region, Germany, Part I: The monazite-(Ce)-brabantite solid solution series. *American Mineralogist, 83*, 259-272.

Gramaccioli C.M., Segalstad T.V., 1978: A uranium and thorium rich monazite from a south alpine pegmatite at Piona, Italy. *American Mineralogist, 63*, 757-761.

Harlov D.E., Wirth R., Hetherington C.J., 2007: The relative stability of monazite and huttonite at 300-900 °C and 200-1000 MPa: Metasomatism and the propagation of metastable mineral phases. *American Mineralogist, 92*, 1652-1664.

Krenn, E., Putz, H., Finger, F. & Paar, W., 2008: Unusual monazite with high S, Sr, Eu and common Pb contents in ore bearing mylonites from the Schellgaden mining district, Austria. *Geophysical Research Abstracts, 10*, EGU2008-A-11796.

Manucci G., Diella V., Gramaccioli C.M., Pilati T., 1986: A comparative study of some pegmatite and fissure monazite from the Alps. *Canadian Mineralogist, 24,* 469-474

Ondrejka M., Uher P., Pršek J., Ozdín D., 2007: Arsenian monazite-(Ce) and xenotime-(Y), REE arsenates and carbonates from the Tisovec-Rejkovo rhyolite, Western Carpathians, Slovakia: Composition and substitutions in the $(REE,Y)XO_4$ system (X = P, As, Si, Nb, S). *Lithos, 95*, 116-129.

Pérez-Soba C., Villaseca C., Orejama D., Jeffries T., 2014: Document Uranium-rich accessory minerals in the peraluminous and perphosphorous Belvís de Monroy pluton (Iberian Variscan belt) Contributions to Mineralogy and Petrology. 167: 1008, 1-25.

Pršek J., Ondrejka M., Bačík P., Budzyń B., Uher P., 2010: Metamorphic-hydrothermal ree minerals in the Bacúch magnetite deposit, western carpathians, Slovakia: (Sr,S)-Rich monazite-(Ce) and Nd-dominant hingganite. *Canadian Mineralogist, 48*, 81-94.

Shannon R.D. 1976: Revised effective ionic radii and systematic studies of interatomic distances in halides and chalcogenides. *Acta Crystallographica, A32*, 751-767.

Terra O., Dacheux N., Clavier N., Podor R., Audubert F. 2008, Preparation of optimized uranium and thorium bearing brabantite or monazite/brabantite solid solutions. *Journal of the American Ceramic Society, 91*, 3673-3682

Uher P., Plašienka D., Ondrejka M., Hraško Ľ., Konečný P., 2013: Uranium-rich monazite-(Ce) from the krivá type granitic cobbles in conglomerates of the Pieniny Klippen Belt, Western Carpathians, Slovakia: Composition, age determination and possible source areas. *Geological Quarterly, 57*, 343-352

Williams M.L., Jercinovic M.J., Hetherington C.J., 2007: Microprobe Monazite Geochronology: understanding geologic processes by integrating composition and chronology. *Annual Reviews of Earth and Planetary Sciences, 35*, 137-175

Chevkinite → allanite reaction relationships in silicic rocks

Silvio RF VLACH[1], Guilherme AR GUALDA[2], Ian M STEELE[3], Frederico CJ VILALVA[4]

[1]*Departamento de Mineralogia e Geotectônica, Universidade de São Paulo, Rua do Lago, 562, 05508-080, São Paulo, SP, Brazil,e-mail: srfvlach@usp.br*
[2]*Department of Earth and Environmental Sciences, University of Vanderbilt, 5726, Stevenson Centre, 7th floor, Nashville, TN 37240, USA, e-mail: g.gualda@vanderbilt.edu*
[3]*Notre Dame Integrated Imaging Facility, Stinson-Remick B10, University of Notre Dame, Notre Dame, IN 46556, USA, e-mail: isteele@nd.edu*
[4]*Departamento de Geologia, Universidade Federal do Rio Grande do Norte, Av. Senador SalgadoFilho, 3000, 59078-970 (PO Box 1639), Natal, RN, Brazil, fredcjv@ufrnet.br*

Allanite and chevkinite are among the most important REE, particularly LREE, carriers in granitic and related rocks and thus control the main LREE budget in many magmatic systems. In the Neoproterozoic 'A-type' Graciosa Province, S-SE Brazil, and in several similar worldwide magmatic provinces, allanite is the typical LREE-rich primary mineral in metaluminous to marginally peraluminous *subsolvus* biotite syeno- and monzo-granites from the so-called aluminous association. In contrast, primary chevkinite is the only LREE-rich primary phase in *hypersolvus* metaluminous to peralkaline alkali-feldspar syenites and peralkaline alkali-feldspar granites from the alkaline association, which was formed in relatively reduced crystallizing conditions. Post-magmatic, hydrothermal, allanite and other epidote-group minerals appear in both associations.

However, in a number of syenitic and granitic varieties from some plutons both primary allanite and chevkinite do appear. Rock textures indicate that allanite crystallized late and substituted for chevkinite, with chevkinite often appearing partially corroded and mantled by allanite (Figure 1); discrete ilmenite grains occur in allanite mantles, suggesting a peritectic-like reaction relationship such as *chevkinite* + $melt_{(1)}$ → *allanite* + *ilmenite* + $melt_{(2)}$. The structure of a crystal fragment from the Farinha Seca Pluton was refined in C2/m [R_1 = 0.0505 for 775 Fo > 4σ(Fo)] and gave **a** = 13.490(3), **b** = 5.757(1), **c** = 11.132(3) [all in Å], **β** = 100.592(4)°, which agrees well with a typical chevkinite unit cell.

These rocks are characterized by structural and textural features which suggest mingling and local mixing processes involving two contrasting magma types, one silicic and the other basic-intermediate. So, in spite of some previous experimental data suggesting that such reaction may be a normal peritectic in a silicic crystallizing system, in the studied cases the geological evidence points to a reaction triggered by mixing processes which change the silicic melt compositions, introducing, among other elements, Ca, Al and Fe.

Similar reaction relationships were observed in a unique sample of peralkaline alkali-feldspar granite collected close to the Papanduva Pluton contacts with older migmatic-gneissic rocks. In this case, however, there is no evidence of mingling; rock magnetic susceptibilities are anomalously high and both textures and associated minerals (*e.g.*, almost pure albite, fluorite) suggest late- to post-magmatic or hydrothermal substitution.

Total REE contents in chevkinite are higher (*ca.* 48-50 wt% oxide) than in allanite (*ca*. 22-27 wt% oxide) but their REE patterns are similar and highly fractionated, with a high fractionation in the LREE range as well as of the LREE over the HREE (*eg*. $2 < La_N/Nd_N < 5$ and Ce_N/Yb_N up to 500) and a strong negative Eu anomaly ($0.02 < Eu/Eu^* < 0.07$). Figure 2 depicts the main gain-loss trends due to the substitution of chevkinite for allanite as determined for an analyzed reaction pair from Sample GRA-16A (Farinha Seca Pluton). This diagram shows that, relative to chevkinite cores, allanite mantles are enriched in Si,

Al, Fe, Ca (and OH-F, not shown), as well as in Mn, Mg, LILE (Rb, Sr, Ba), Zn, Sn and Pb; allanite mantles are depleted in Ti and also P, Ga, HFSE (Zr, Hf, Nb, Ta), Mo, REE (especially the HREE, Sc and Y), Th and U. These characteristics may be accounted for by a basic-intermediate input into silicic melts and partial mixing as well as by the interaction of primary chevkinite with relatively Ca-, Al- and Fe-rich late- to post-magmatic fluids.

In silicic systems, allanite is a stable mineral in magmatic and hydrothermal environments, so it may substitute for chevkinite in both situations, depending only on the composition of the reference system, including (OH) activity. It is difficult to precisely evaluate the fO_2 effect, but it is suspected that allanite is favored by relatively high oxidizing conditions.

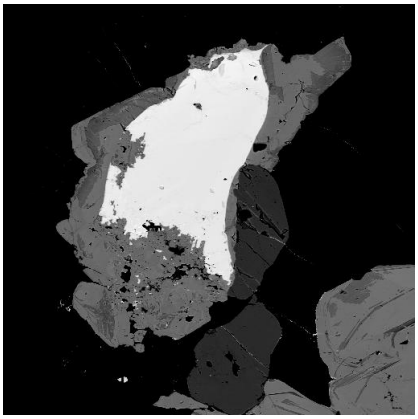

Fig. 1. BSE image showing a typical mantle texture involving chevkinite and allanite. Sample 16A, syenite, Farinha Seca Pluton, Graciosa Province.

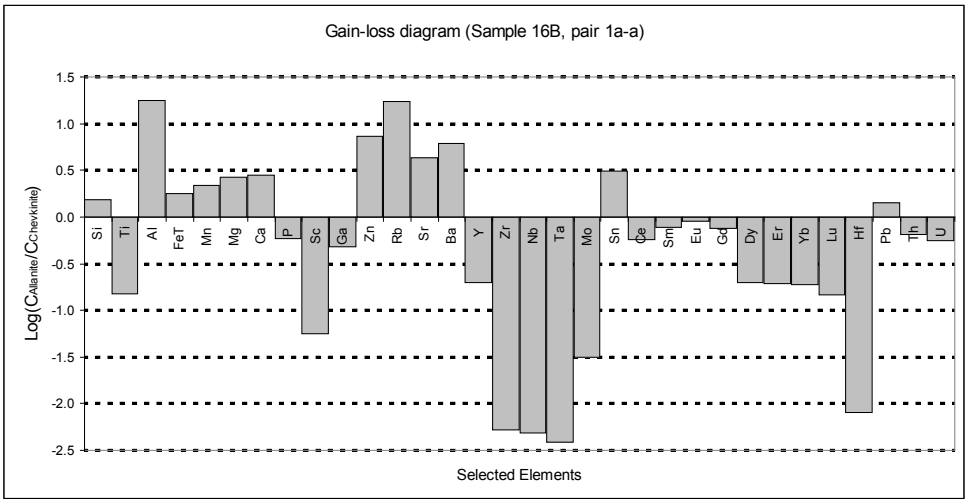

Fig. 2. Elemental budget due to the substitution of chevkinite for allanite (EPMA and LA-ICPMS data). Sample GRA-16B, syenite, Farinha Seca Pluton, Graciosa Province.

Structural and electron density X-ray investigations beyond independent atom approximation

Krzysztof WOŹNIAK, Marcin STACHOWICZ

Chemistry Department, University of Warsaw, Pasteura 1, 02-093 Warszawa, Poland.
E-mail: *kwozniak@chem.uw.edu.pl*

Although everything seems to be already well known in the field of routine structural single crystal X-ray analysis, even commonly used approaches and models should be critically re-evaluated. The most common model of electron density used in X-ray studies which is based on spherical atoms –the Independent Atom Model (IAM) – was introduced about a century ago. It was then adequate, when the very poor quality of the hardware was introducing far bigger errors in the experimental data than the applied model of electron density. Now, however, when modern diffractometers and synchrotron stations allow us to collect very high quality X-ray and neutron diffraction data, the quality of the model of electron density used in structural refinements may be, and should be, increased by taking into account the aspherical distribution of atomic electron densities. The main ideas of methods going beyond IAM, such as the experimental multipole model of charge density and Hirshfeld Atom Refinement (HAR), will be presented. The accuracy and precision of structural data obtained from multiple routine measurements, charge density studies and HAR will be discussed. It will be shown how structural parameters such as bond lengths and valence angles are dependent on the 2 theta diffraction angle. Some practical suggestions will be presented on how to estimate and improve the quality of single crystal X-ray diffraction structural results. A comparison of geometrical parameters obtained from routine low resolution, charge density high resolution single crystal X-ray studies and HAR will be discussed. Also some new applications of experimental charge densities - including minerals - showing their potential will be presented.

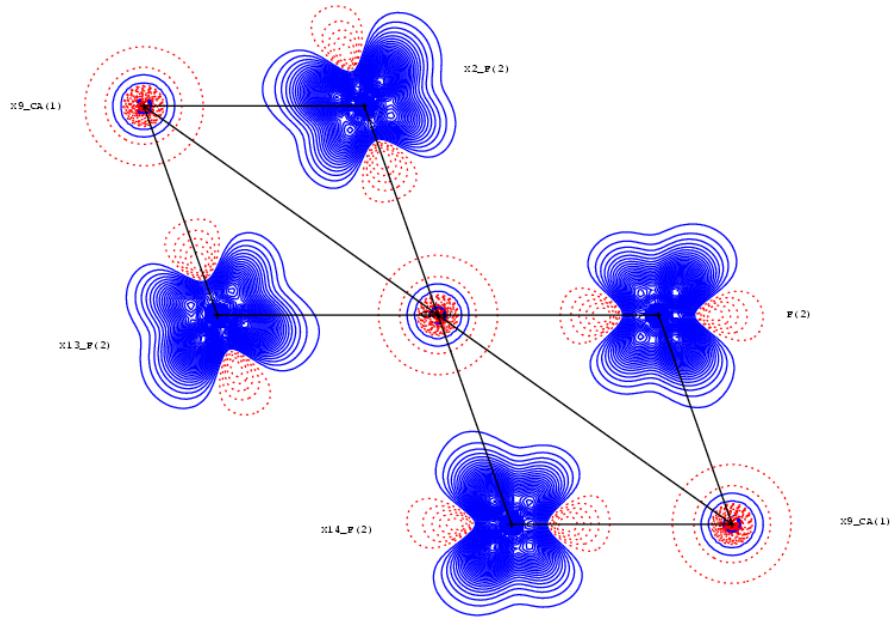

Fig. 1. Aspherical distribution of electron density in Fluorite.

Genesis and alteration mechanisms of britholite group minerals from ore bodies related to the Keivy peralkaline granite-nepheline syenite complex, Kola Peninsula, NW Russia

Dmitry ZOZULYA[1], Lyudmila LYALINA[1], Ray MACDONALD[2], Bogusław BAGIŃSKI[2], Yevgeny SAVCHENKO[1], Piotr DZIERŻANOWSKI[2]

[1]*Geological Institute, Kola Science Center, Russian Academy of Sciences, 184209 Apatity, Russia; zozulya@geoksc.apatity.ru*
[2]*Institute of Geochemistry, Mineralogy and Petrology, University of Warsaw, 02-089 Warsaw, Poland*

The Late Archean Keivy peralkaline granite-syenite complex consists of aegirine-arfvedsonite granites (six sheet-like massifs of a few hundred meters thickness and a total exposure area of ca. 2500 km^2), aegirine-augite-lepidomelane-ferrohastingsite syenogranites that occur in the margins of some massifs, and lepidomelane-ferrohastingsite syenite dykes that intrude the TTG basement of the Central Kola terrane (NE Fennoscandian shield, Kola Peninsula). Small dike-like bodies of nepheline syenite cut the West Keivy peralkaline granite massif. On standard trace element discriminant diagrams (Pearce *et al.* 1984, Whalen *et al.* 1987, Eby 1990) the Keivy peralkaline granites plot as within-plate or post-collisional A-type granitoids. The low Y/Nb and Yb/Ta ratios for the associated nepheline syenite indicate an OIB affinity. The rocks of the Keivy complex are extremely enriched in Zr (300-5000 ppm), Y (40-500 ppm), Nb (20-600 ppm), Rb (160-900 ppm), REE (100-1000 times chondrite), which is explained by an enriched mantle source for the primary melts and extreme fractionation processes. The numerous associated Zr-Y-REE-Nb ore occurrences and deposits are associated with different lithologies and were formed by different genetic (late- and post-magmatic) processes: mineralized apical and veined granites, mineralized nepheline syenites, quartzolites (silexites), various metasomatic rocks, pegmatites.
Britholite group minerals (BGM) are found as accessory minerals in all types of granites and syenites and form major and ore-forming phases in quartzolite, mineralized nepheline syenite, nepheline-feldspar pegmatite.

BGM in quartzolite

Abundant BGM are revealed in quartzolite bodies, confined to apical parts of peralkaline granite massifs, their content reaching 5-10 vol%. Three morphological types of BGM are distinguished in quartzolite-1 (endocontact zone): (1) subhedral (most abundant) grains up to 1-2 cm; (2) anhedral grains in intergrowths with yttrialite-(Y); (3) poikilitic crystals and skeleton aggregates. All types are represented by fluorbritholite-(Y) and are characterized by unusually low phosphorus content with successive decreasing of the P_2O_5 content (from 5-1 wt% in type 1) down to formation of the phosphorus-free silicate fluorbritholite-(Y) in types 2 and 3. Type 1 crystals show inter-phase heterogeneity: the phosphorus content decreases and the HREE content increases from internal to outer zones. The total REE content increases insignificantly from 1 to 2 morphotypes and drastically decreases in fluorobritholite-(Y) of type 3. The successive domination of HREE over LREE during this process points to hydrothermal conditions of mineral crystallization from a F-rich and P-poor fluid. BGM from quartzolite-1 have a thin alteration rim which is composed of an X-ray amorphous substance with lower Ca and Y contents and with inclusions of monazite and bastnäsite. BGM in quartzolite-2 (exocontact zone) are represented by fluorbritholite-(Y) with higher P_2O_5 (3.1-7.7 wt%) and LREE, and lower Y contents compared to BGM from quartzolite-1. This can be explained by contamination of the fluid leading to a decrease of alkalis and fluorine activity.

BGM in mineralized nepheline syenite

BGM are the main ore minerals in REE-Zr deposits related to the nepheline syenite massif, their grade varying from 0.2 to 1 vol%. They are represented by individual (up to 1 mm) subhedral and anhedral crystals (in lepidomelane-aegirine syenite) and by large (up to 20 mm) aggregates of grains (in recrystallized amphibole syenite). The mineral often includes "porous" zircon, fluorite and albite, which points to a late- and post-magmatic origin. Fluorbritholite-(Ce) is the most abundant mineral species and occurs in both rock types. From the mineral associations and REE chemistry (f.e. La/Nd_n = 4.4-6.4) it is suggested that fluorbritholite-(Ce) crystallized during albitization from an alkali- and F-rich and CO_2-bearing fluid. Britholite-(Ce) and fluorbritholite-(Y) are present only in amphibole syenites. They are characterized by lower La/Nd_n ratio (2.8-3.8) and higher Th content that may indicate crystallization from aqueous and F-bearing, but CO_2-free, fluid. BGM from nepheline syenites are altered, with the formation of lower Z patches and rims and release of F, Ce, La. A possible reaction for rim formation is britholite + fluid → apatite + epidote + REE carbonate.

BGM in nepheline-feldspar pegmatite

The unique diversity of the BGM is established in a nepheline-feldspar pegmatite related to the contact zone between nepheline syenite and essexite: fluorbritholite-(Ce), britholite-(Ce), fluorbritholite-(Y), fluorcalciobritholite and hypothetical phases "calciobritholite" and "fluorbritholite-(La)". BGM form two morphological types: (1) individual euhedral prismatic crystals of 1.5-2 mm length and (2) anhedral grains up to 8-10 mm size. Often, intergrowths of apatite and fluorite are found, inferring high activities of F and P during BGM formation. Pegmatitic BGM differ from nepheline syenitic occurrences in lower Pr, Nd, Sm. The chondrite-normalized REE pattern has a U-shape form with enrichment in the lightest and heaviest REE. "Calciobritholites" contain much lower LREE, Gd, Tb, Dy, Ho compared to cerian and yttrian "britholites" from the same pegmatite. La/Nd_n ratio varies in the range 8-10, indicating high CO_2 activity in the pegmatitic melt/fluid. Alteration rims of pegmatitic BGM are characterized by lowering of Z and formation of apatite grains, suggesting the release of REE.

Conclusions

Britholite group minerals from ore bodies related to a Keivy peralkaline granite-nepheline syenite complex, Kola Peninsula, NW Russia, were formed predominantly during the late- and post-magmatic stages. The diversity of BGM species and their compositional ranges point to the sensitivity of BGM to the species and composition of fluids in the crystallization media. Post-crystallization alteration led mainly to release of REE.